IEEE Access
Multidisciplinary ⋮ Rapid Review ⋮ Open Access Journal

Received 8 July 2025, accepted 28 July 2025, date of publication 1 August 2025, date of current version 8 August 2025.

Digital Object Identifier 10.1109/ACCESS.2025.3594845

RESEARCH ARTICLE

Optimized and Routed Wiring Harness Based on Zonal Clustering Concept Using AI in the Automotive Industry

MD SANOWAR HOSSAIN, HAFIZ ABDUL QUDDUS, ZIYA CEVAHIR, AND ALEXANDER JESSER
Institute for Intelligent Cyber-Physical Systems (ICPS), Heilbronn University of Applied Sciences, 74653 Künzelsau, Germany

Corresponding author: Md Sanowar Hossain (md-sanowar.hossain@hs-heilbronn.de)

This research is funded by the German Federal Ministry of Education and Research (BMBF) under grant number 16ME0783, within the KI4BoardNet project (''Integral Agile E/E Development for Fusion and Standardized Power and Data Wiring Systems'') as part of the funding initiative ''Electronics and Software Development Methods for the Digitalization of Automobility.''

ABSTRACT This paper presents an AI-driven approach for multi-zonal clustering and harness routing optimization in automotive electrical/electronic (E/E) systems. A methodology integrating K-means clustering with dynamic grid-based routing algorithms (A* and Bresenham's line algorithm) is applied to optimize the wiring harness layout across the vehicle's zones, covering six key domains (comfort, chassis, drive assist, infotainment, system, and powertrain). The proposed method accounts for realistic vehicle constraints, including restricted zones and diverse wire types, which are often overlooked in prior work. A 12-Zone architecture under a high application-load scenario is examined, demonstrating that this configuration achieves an optimal trade-off between harness length, complexity, and cost efficiency. Compared to manual design approaches and existing zonal architectures in the literature, the AI-based method reduced design time, produced a leaner harness layout, and achieved measurable material and cost savings. Specifically, the 12-Zone cluster arrangement achieved a total wiring distance of 241.056 m and a total wire mass of 22.92 kg for 417 ECUs, outperforming both lower and higher zone counts in overall efficiency. Scalability tests from 1 to 14 zones (under Low, Mid, and High load variants) confirmed the robustness of the approach and identified the 12-Zone configuration as the best-balanced solution. These findings highlight the potential of AI-optimized zonal E/E architectures to significantly reduce wiring weight, complexity, and design effort while maintaining system performance and cost competitiveness, providing valuable insights for next-generation automotive E/E design.

INDEX TERMS A* algorithm, automotive electrical/electronic (E/E) architecture, Bresenham's algorithm, clustering algorithms, grid-based routing, high-performance computer (HPC), in-vehicle network topology, machine learning, K-means clustering, ring topology, routing algorithms, system integration, wiring harness optimization, zonal architecture.

I. INTRODUCTION

In the rapidly evolving landscape of autonomous and electric vehicles, the complexity and interconnectivity of electronic systems have grown exponentially. At the core of these systems lies the wiring harness—a structured assembly of wires, connectors, and terminals responsible for power and data communication throughout the vehicle. As vehicle functionalities become increasingly sophisticated, the demand for optimized, lightweight, and cost-effective harness architectures is intensified. Traditionally, the design and routing of wiring harnesses are carried out manually or through conventional Computer-Aided Design (CAD) tools [1]. While these methods provide a foundational basis, they are often time-consuming, labor-intensive, and offer limited scalability and optimization.

Industrial partners such as EDAG and KROSCHU, active participants in the KI4BoardNet project, currently rely on

The associate editor coordinating the review of this manuscript and approving it for publication was Valentin Ivanov.

manual processes or CAD-based techniques for wiring harness design. These methods result in extended development cycles, high labor costs, and suboptimal resource allocation, achieving only about 50% cost-efficiency compared to potential computational techniques. The shift from traditional domain-based electrical architectures to zonal architectures in autonomous vehicles demands a rethinking of harness design strategies. This transformation has given rise to the Zonal Clustering concept, which groups components based on physical and functional proximity, offering a promising approach for streamlining wiring layout and routing.

The rationale for this study lies in leveraging Artificial Intelligence (AI) to automate and optimize the design and routing of wiring harnesses based on the Zonal Clustering concept. Despite the growing availability of machine learning tools and computational geometry algorithms, a significant methodological gap persists in current automotive design research. Prior studies have not sufficiently explored AI-based frameworks for harness optimization within zonal electrical architectures. Furthermore, empirical evaluations of such frameworks, particularly in collaboration with industrial stakeholders like EDAG and KROSCHU, remain scarce. This study aims to fill these gaps by proposing and validating a novel, AI-driven system for harness clustering and routing.

The main objective of this research is to develop an optimized and routed wiring harness framework based on Zonal Clustering using AI, specifically tailored for the autonomous automotive industry. The specific objectives include: (i) designing AI-based clustering and routing models for power and data communication harnesses, (ii) minimizing harness weight while ensuring routing feasibility, and (iii) validating the system under real-world industrial constraints.

The researcher identified a methodological gap in the prior research. There is a lack of AI-based clustering and routing research designs in the automotive harness optimization domain. Based on the research implemented, there is a dearth in prior studies on hybrid optimization and context-aware routing design. This study seeks to establish a new inquiry by introducing Dynamic Grid Adaptation, Restricted Zone-Aware Optimization, and hybrid routing protocols. It extends current research by addressing gaps through empirical validation with industry partners, implementing multi-algorithmic fusion in research methodology.

This study offers several novel contributions: Dynamic Grid Adaptation automatically adjusts resolution based on local component density; Restricted Zone-Aware Optimization introduces dual-phase handling of routing constraints; Hybrid Routing Protocol combines algorithms such as A* and Bresenham's to ensure context-aware path selection; and Weighted Metric Fusion integrates geometric and electrical constraints to enhance optimization quality. The final analysis indicates that harness weight distribution varies across application tiers—Low, Mid, and High—but remains within practical and feasible limits. This approach enables the development of lightweight, efficient, and scalable electrical architectures in modern vehicles.

Historically, the automotive industry has relied on manual methods for wiring harness design, often involving iterative 2D layouts and basic CAD systems. While effective for simpler architectures, these methods lack the scalability and intelligence needed for zonal-based autonomous systems. Recent research has made strides toward automation, but comprehensive AI-driven frameworks remain underexplored, particularly those that integrate clustering, routing, and empirical validation in industrial settings.

The rest of this paper is structured as follows: Section II reviews related literature on harness design, clustering methods, and AI applications in automotive systems. Section III presents the proposed methodology, including algorithmic design and optimization strategies. Section IV details the experimental results and discussions, including industry-level validation. Section V concludes the research with final insights and suggestions for future work. The last section contains the references cited throughout this study.

A. ABBREVIATIONS AND ACRONYMS

High-Performance Computer (HPC), K-Dimensional Tree (KDTree), Restricted Zone (RZ), Flexible Low-Tension Reduced-Weight Cable (FLRY), Power Supply (P.Supply), Nominal Power (NP), Artificial Intelligence (AI), Dynamic Programming (DP), Automatic Wire Routing (AWR), Application Variant (AV), Electric Vehicle (EV), Pathfinding Algorithm (PFA), EDAG Engineering GmbH, KROSCHU (Kromberg & Schubert Automotive GmbH & Co. KG), Electronic Control Units (ECUs), In-Vehicle Network (IVN), Domain-based IVN architecture (DIA), zone-based IVN Architecture (ZIA).

II. RELATED WORK

Autonomous vehicles (AVs) demand flexible and intelligent electrical/electronic (E/E) systems. Traditional domain-based wiring is no longer optimal due to complexity and weight. Zonal architecture, enhanced by AI, enables efficient design, routing, and scalability.

A. ZONAL ARCHITECTURE AND OPTIMIZATION TECHNIQUES

Maier and Reuss [2] proposed a hybrid algorithm that combines K-means clustering with Dijkstra's algorithm for forming efficient zonal E/E architectures. A second study [3] evaluates zonal design complexity through simulation. Hybrid zonal-domain networks improve performance and reduce wiring [4]. Robotics-based zonal systems also show physical and weight reductions [5]. Lim et al. [6] developed a framework for designing zonal architectures that effectively balance communication load and wiring length, addressing key trade-offs in modern E/E systems. Kadry et al. [7] provided a comprehensive review of challenges and future trends in electrical architecture and in-vehicle networking,

emphasizing the shift towards zonal concepts and the implications for optimization techniques.

B. AI-BASED HARNESS DESIGN AND ASSEMBLY

Gopinath and Thenmozhi [8] utilized AI for connector selection, streamlining design workflows. Arvind [9] introduced a simulator for pigtail harness development using intelligent configuration systems. Karlsson et al. [10] developed a 3D modeling tool that automates harness placement using AI-driven layout assistance. Prabhakaran et al. [11] designed and developed an intelligent zone-based primary electronic control unit (ECU) for power optimization in electric vehicles, demonstrating how zonal clustering and AI integration can improve efficiency and adaptability in harness design.

C. ROUTING ALGORITHMS

A* pathfinding is widely applied for shortest path routing in AVs [12], [13]. B-spline optimization enhances collision-free routing [14]. Kim and Lee [15] developed a B-spline and pathfinding hybrid method to avoid physical interferences during cable layout. Similarly, Liu et al. [16] applied the A* search algorithm for chassis-level harness optimization. Gaon et al. [17] employed K-means clustering and genetic algorithms to optimize electric vehicle routing efficiency, presenting a novel methodology that can also inform efficient harness routing and layout decisions.

D. AI IN CLUSTERING AND DECISION-MAKING

Neural networks and attention mechanisms improve perception and routing [18], [19]. Clustering in VANETs enhances secure communication [20], [21].

E. AUTOMATION AND ROBOTICS

In harness manufacturing, Wang and Johansson [22] implemented a deep learning-based robotic system for detecting and assembling cable connectors. Wu et al. [23] proposed attention-enhanced path planning algorithms, applicable to smart harness routing around 3D obstacles. Robotic harness tracing automates production [24].

F. SIMULATION AND TOOL-BASED DESIGN

Simulation-optimized E/E design supports performance-cost balance [25], [26]. CAD tools aid visual EV harness layout [27]. Graph-based models optimize flow configurations [28].

G. PERFORMANCE AND NETWORK SIMULATIONS

Park et al. [29] evaluated E/E communication delays in zonal in-vehicle networks, showing a balance between reduced cable length and latency. Bianchi et al. [30] combined simulation and mixed-integer optimization to evaluate off-road E/E network topologies.

H. IN-VEHICLE COMMUNICATION

Zonal IVNs reduce wiring and latency [31], [32]. OFDMA-based Ethernet improves data throughput [33]. Selective data distribution cuts communication delay [34]. AI-driven IDS enhances Ethernet security [35].

I. ZONAL AI ARCHITECTURE AND OUTLOOK

AI and edge computing enable smart zonal diagnostics and control [36]. Clustering helps in behavioral anomaly detection [37]. Shetiya et al. [38] described an AI-enhanced zonal architecture that integrates diagnostics and distributed intelligence, aligning with future AV requirements for modular and scalable systems. Bornemann [39] outlined the potential of zone controllers as a bridge to future E/E architectures, emphasizing benefits in wiring reduction and modularity for next-generation vehicles. Aberl et al. [40] elaborated on how zonal architectures support fully software-defined vehicles, with AI playing a role in configuration and dynamic adaptation of the E/E system. Nguyen et al. [41] proposed automation strategies for harness production using AI, and Askaripoor et al. [42] recommended AI-based clustering and optimization to meet E/E design complexity and reliability challenges. Larrenie et al. [43] proposed ML-based latency prediction for automotive networks to inform optimal zonal harness routing.

The reviewed literature underscores the significant progress made in optimizing vehicle wiring harness systems through zonal architecture and Artificial Intelligence. Hybrid clustering techniques, intelligent routing algorithms, and automation-driven assembly processes have collectively advanced the design of electrical/electronic (E/E) architectures. Nevertheless, several limitations persist across existing state-of-the-art approaches.

Firstly, many clustering techniques, including those based on K-means or neural networks, often overlook physical constraints such as restricted zones, heat-sensitive areas, or mechanical boundaries within vehicle platforms. Most studies also focus on static or uniform grid resolutions, lacking the capacity for Dynamic Grid Adaptation that can tailor spatial resolution based on component density or design complexity. While AI-based routing methods like A* and B-spline optimization have shown effectiveness, few integrate dual-phase routing logic that differentiates between open zones and restricted pathways.

Moreover, although data-driven methodologies are gaining traction, there is a noticeable lack of implementation using real-world industrial datasets. Most simulations are based on synthetic or idealized layouts, leading to limited generalizability. Additionally, little attention has been paid to optimizing both power and data communication harnesses simultaneously, especially across varying application tiers such as low-, mid-, and high-complexity configurations. Current solutions often treat wiring harness optimization in isolation without addressing the holistic integration of functional, spatial, and electrical design constraints.

To address these challenges, this research proposes a novel framework that integrates Zonal Clustering and AI-powered routing algorithms with real-world constraints. The direction of this study includes: (i) routing harnesses by intelligently

avoiding restricted or prohibited zones using spatial analysis and obstacle-aware algorithms; (ii) implementing Dynamic Grid Adaptation for scalable resolution control based on local component density; (iii) optimizing harnesses for both power and data communication pathways; and (iv) evaluating performance across multiple vehicle application levels (low, mid, high) using a unique industrial dataset provided by project partners such as EDAG and KROSCHU.

By addressing the identified gaps, this study seeks to establish a new standard for intelligent, adaptive, and empirically validated wiring harness design in the context of zonal architectures for autonomous vehicles.

III. MATERIALS AND METHODS

A. DATASET OVERVIEW

This study employs a detailed and structured dataset obtained from the KI4BoardNet project, hosted by edacentrum [44]. The dataset was developed through industrial collaboration with partners such as EDAG and KROSCHU, and represents a comprehensive set of real-world wiring and component data used in the design of automotive zonal electrical architectures. It serves as the foundation for implementing clustering, routing, and optimization techniques using Artificial Intelligence (AI).

The dataset contains 11,988 unique component indexes across 59 structured features, which include component attributes, spatial positioning, electrical parameters, wire specifications, and constraint zones. Components span a wide range of automotive domains such as Infotainment, Comfort, Chassis, Powertrain, Drive Assistance, System, and Body. Each domain is further categorized into sub-domains, such as User Media, Communication, Power Window, Internal Illumination, Automated Driving, Battery Cooling, and Park Assistance.

1) COMPONENT-LEVEL DATA REPRESENTATION

The dataset includes a wide range of component types essential to automotive electrical systems, such as Actuators, Switches, Sensors, Igniters, Cameras, Antennas, Control Units, Noise Filters, DCDC Converters, Loudspeakers, Inlets, Interface Connectors, Relays, Power Distributors, Radars, and Lidars. In total, there are 843 distinct components, including critical elements such as the Airbag – Driver Module, Rear View Camera, CO_2 Detection – Air Quality Sensor, Navigation – GPS Antenna, Computing – WiFi Unit, 12 V Battery, Wiper Motor, and many others. Each component is associated with a coordinate reference, representing its precise spatial location within the vehicle layout. These coordinates are fundamental for path planning and harness routing decisions. Additionally, connections to zone Controllers are defined for both power and signal lines. The field Wire Gauge [mm^2] provides recommended cable types at industry standards (e.g., FL09YBCY 4 × 0.50+SCHIRM, FLRY 2 × 0.13, RG174), specified under 85°C and 12 V conditions.

The dataset also supports analysis across application tiers—Low, Mid, and High —allowing researchers to simulate routing and performance impacts under different levels of vehicle complexity.

A representative subset of the component records is presented in Table 1, showcasing component indices, coordinates, pinout configurations, zone controller connections, and boardnet wire specifications.

TABLE 1. Representative excerpt from the component dataset used for routing simulations. Each entry includes the component's spatial coordinates, pinout configuration, power supply requirement, signal usage, nominal power consumption, and associated wire gauge type. This data serves as input to the clustering and routing algorithms.

Index	Coord.	Pinout	P.Supply	Signal	N.Power[W]	Wire Gauge
1	35;0	1	Yes	Yes	0.7	FL09YBCY
8	36;0	A2	No	Yes	0.0	RG174
30	38;-21	1	Yes	No	0.6	FLRY 0.13
36	32;-22	1	No	No	48.0	FLRY 0.50
49	44;-15	3	No	No	36.0	FLRY 0.35
92	108;-17	5	Yes	No	18.0	FLRY 0.35
83	28;-6	6	No	Yes	0.6	FLRY 0.13
8	36;0	1	Yes	No	12.0	FLRY 0.13
8	36;0	3	No	Yes	0.2	FLRY 2x0.13

2) RESTRICTED ZONES AND ROUTING CONSTRAINTS

The dataset includes a Restricted Coordinates section that flags spatial regions in the vehicle architecture that are off-limits for wiring—such as engine blocks, high-heat zones, and structural barriers. These constraints are fed into the routing algorithms (e.g., A*, KDTree) to ensure practical, feasible harness paths that mimic real-world engineering rules.

3) WIRE CHARACTERISTICS AND HARNESS WEIGHT MODELING

The most recent and detailed part of the dataset is in the Wire Characteristics Table 2, which defines key electrical, physical, and environmental parameters in accordance with ISO 19642-4, ISO 19642-3, and ISO 6722-1 automotive standards. Each wire is listed with a unique code (e.g., FLRY 0.22), along with its description, material type, and electrical properties. These attributes are essential for calculating both individual cable segment weights and total zonal harness weight. Such characteristics are critical in evaluating the effects of design changes on overall weight, performance, and efficiency.

Table 2 presents a sample of wires and cables used in the harness system, highlighting the Boardnet Wire Gauge, standard compliance, wire carying capacity[A] and total weight per meter. These wires are used to connect zonal centroids to component locations, batteries, and High-Performance Computers (HPCs), enabling accurate modeling of both cluster-level and total harness weight.

This wire-specific data is fully integrated into the simulation and optimization pipeline to support accurate weight modeling along each routing path. These insights directly influence zonal clustering strategies and AI-based routing decisions. The dataset's high fidelity, standardized attributes,

and adaptability across application tiers make it well-suited for validating advanced harness optimisation methodologies in zonal vehicle architectures.

TABLE 2. Reference wire types and specifications used in zonal harness weight estimation. Values are based on ISO automotive wire standards and include the wire gauge designation, applicable standard, current-carrying capacity, and wire weight in grams per meter. These parameters are used to calculate zone-wise harness weight in the proposed approach.

Wire Gauge	Standard	WireCaryingCapacity[A]	Wire Weight [g/m]
FLRY 0.22	ISO 19642-3	4.98	3.20
FLY 120.00	ISO 19642-3	279,56	1240
FLRY 0.35	ISO 19642-3	6.67	4.26
FLRY 35	ISO 19642-3	351	1446.20
FLY 1.50	ISO 19642-3	17.28	20.00
FLY 6.00	ISO 19642-3	42.88	68.00
FLR2X 0.35	ISO 6722-1	8.60	3.00
FLY 0.50	ISO 19642-3	8.57	8.0
FLR2X 1.00	ISO 6722-1	13.64	13.00
FLRY 8.00	ISO 19642-3	52.30	77.00

B. DATA PREPROCESSING, FEATURE ENGINEERING, AND FEATURE SELECTION

1) DATA PREPROCESSING

Data is first imported from the provided sources, which included the component dataset (Table 1) and the wire characteristics dataset (Table 2). This ensured that all relevant raw information is available for analysis. After loading, the combined data is filtered by application type (Low, Mid, High) to restrict the scope to the relevant categories. Filtering by these application labels focuses the analysis on comparable groups of components, thereby improving consistency and relevance of subsequent modeling.

Next, the dataset is validated for completeness of essential columns. All required attributes (such as connection flags and coordinate fields) are checked for presence and correct formatting. This validation step is important to prevent missing or malformed data from causing errors downstream. Ensuring that key columns exist and are properly formatted guarantees that later computations (e.g., weight calculations or spatial analysis) have the necessary inputs. Uniform data types are then enforced for quantitative fields. Numerical values that had been stored as strings in the raw data (notably some wire weight parameters) are converted into proper numeric format. In particular, the wire weight-per-unit-length attribute (given in g/m) is parsed from text to a float value. Converting these string-encoded numbers to numeric types is essential for allowing mathematical operations (such as computing total wire weight) and avoiding misinterpretation of what should be quantitative data.

Spatial information in the component dataset is also standardized. Coordinates provided as a single string are parsed into separate numeric x and y values for each component's location. This parsing makes the positional data readily usable for calculations like distance or spatial clustering. By splitting coordinates into numeric fields, spatial relationships and routing calculations (for instance, determining wire lengths or proximity to obstacles) can be handled with precision in later analysis.

Irrelevant or non-connected entries are removed to refine the dataset. Any component indicated as having no power supply connection and no signal connection (i.e., both flags set to "No") is considered isolated and is excluded. Eliminating these non-connected components is important because they do not participate in the electrical network and would not influence connectivity or routing outcomes. Their removal reduces noise in the data and ensures that subsequent processing focuses only on meaningful, connected components. Additionally, duplicate records are identified and dropped, guaranteeing that each physical component or connection appears only once. Removing duplicates preserves data integrity and prevents any single component from inadvertently skewing the analysis due to multiple entries. Finally, records with missing key values are discarded. Entries lacking critical information (such as missing coordinates, unspecified connection type, or other essential attributes) are dropped because incomplete data can undermine the accuracy of feature calculations and model training. By removing records with missing fields, the dataset's overall quality and reliability are improved before feature derivation. In parallel, a separate dataset containing restricted area information (routing obstacle zones) is loaded and parsed. The coordinates delineating each restricted zone are extracted into usable numeric form, analogous to the component coordinates. This step ensures that physical routing constraints are captured in the data preparation stage, enabling their incorporation into later feature engineering and modeling steps.

2) FEATURE ENGINEERING

Based on the cleaned dataset, new features are derived to capture important characteristics of the wiring system. One key engineered feature is the wire weight for each connection. Using each wire's length and its specific weight-per-unit-length (from the attributes in Table 1 and Table 2), the total weight of that wire segment is calculated. This computed wire weight provides a quantitative measure of material mass for each connection, which is a critical factor in harness design constraints (influencing both mechanical load and cost considerations). Including wire weight as a feature allows the analysis to account for the impact of different wire lengths and gauges on overall system weight.

Spatial features are also formulated to leverage the coordinate information. With each component's x and y coordinates available, it became possible to derive distance-based features. For example, the geometric distance between connected components can be calculated to approximate wire routing lengths if not provided directly. Furthermore, the distance of any component or wire segment to the nearest restricted area can be evaluated using the parsed obstacle coordinates. Such a feature would indicate how close a given connection comes to a no-go zone, reflecting routing difficulty. By engineering these spatial features, the model can incorporate the physical layout of components and

identify potential design conflicts or complexity due to spatial constraints.

Connectivity-related features are constructed from the boolean flags present in the data. The binary indicators for power supply connection and signal connection are directly used as features to represent each component's connectivity status. These flags can also be combined to categorize the role of a component (for instance, distinguishing between power distribution nodes, signal-only nodes, or fully connected nodes). Capturing the connectivity state in a feature is important because it conveys the functional significance of a component within the network, which may correlate with different design rules or risk factors (e.g., power nodes might require heavier gauge wires). By including these as features, any modeling process can differentiate components by their electrical role.

Additional domain-specific features are considered as well. The application type (Low, Mid, High), already used for filtering, can be retained as a categorical feature to inform the model of the context or operational class of each instance. In practice, this categorical feature would be encoded (for example, via one-hot encoding or ordinal encoding) so that it can be utilized by machine learning algorithms. Similarly, if there are categorical descriptors of wires (such as insulation material or standard code from Table 1), these can be transformed into feature variables. Every engineered feature is chosen to reflect a meaningful aspect of the wiring harness problem—whether physical (length, weight, spatial position) or logical (connectivity type, application category)—ensuring that the feature set richly represents the factors that could influence outcomes in the subsequent analysis.

3) FEATURE SELECTION

After engineering the candidate features, a feature selection process is applied to identify the most relevant subset for modeling. In this step, any features that are not informative for the predictive objectives or that are redundant are removed. First, non-informative attributes such as purely descriptive text fields or identifiers (e.g., component codes or names used only for labeling) are excluded, since they do not contribute to the predictive modeling and could introduce noise. This focuses the analysis on quantitative and categorical features with potential impact.

Next, the remaining features are examined for redundancy and multicollinearity. If two features are highly correlated or one is derivable from another, one of them is pruned. For instance, if both wire length and wire weight are present as features, one might be dropped because wire weight is directly computed from length (given a fixed weight per unit length). By removing such collinear features, the feature set avoids duplicating information, which simplifies the model and prevents instability in model coefficients. Additionally, features with very low variance (nearly constant values across all data points) are eliminated, as they carry little information

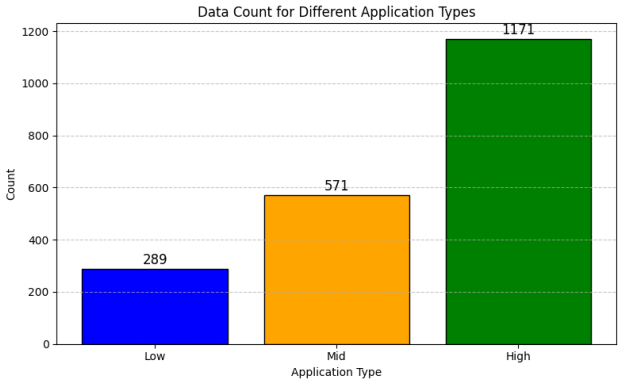

FIGURE 1. Number of retained features after preprocessing for Low (289), Mid (571), and High (1171) vehicle application tiers.

and can safely be excluded without harming the model's performance. This step improves the signal-to-noise ratio in the data by discarding attributes that do not differentiate between instances.

In some cases, domain knowledge and iterative testing guided the selection of the final features. Features known to have strong influence on the outcome (for example, those related to physical constraints like weight or critical connectivity indicators) are prioritized, whereas less significant ones are dropped. If an automated feature importance ranking or statistical test is employed, it would further ensure that only features with substantive predictive power are retained. The result of this feature selection stage is a refined set of input variables that are both relevant and non-redundant. Fig. 1 illustrates the processed dataset after applying feature selection and feature engineering.

4) APPLICATION SCENARIOS AND RETAINED COMPONENTS

To enable meaningful comparison with prior work, the dataset is preprocessed and reduced through feature selection, yielding distinct subsets for each application tier. Specifically, the feature selection retained 103, 206, and 417 components for the Low, Mid, and High application scenarios, respectively. These subsets are then used in the routing simulations and subsequent evaluation of performance metrics, as detailed in Section IV.

5) BASELINE WIRING HARNESS TOPOLOGY

Fig. 2 presents the baseline wiring harness structure applied to Low, Mid, and High application tiers. The layout illustrates the complete connection hierarchy—ranging from Components-to-Centroids wiring, inter-centroid (ring) communication paths, Centroids-to-HPC (High-Performance Computer) links, and Centroids-to-Battery routes. This configuration serves as the reference model against which the automated harness generation framework is evaluated in terms of layout accuracy, routing efficiency, and weight optimization.

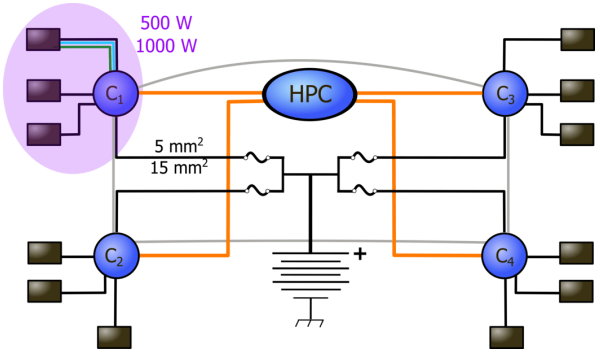

FIGURE 2. Baseline wiring harness topology used across application tiers.

C. METHODS

1) K-MEANS CLUSTERING FOR HARNESS ZONE OPTIMIZATION

K-means [45] clustering is used to partition components into spatially compact groups (clusters) based on their grid coordinates. Given a desired number of clusters k, the algorithm iteratively minimizes the within-cluster sum of squared distances:

$$\arg\min_{C} \sum_{i=1}^{k} \sum_{x \in C_i} \|x - \mu_i\|^2 \tag{1}$$

where C_i represents the set of points in cluster i and μ_i is the centroid. In the context of harness design, centroids are used as routing hubs to reduce total wiring length.

Algorithm 1 Simple K-Means Algorithm

Input: Dataset X, number of clusters k
Output: k optimized clusters with centroids

1: Randomly initialize k centroids from data points in X
2: **repeat**
3: **for all** points $x_i \in X$ **do**
4: Assign x_i to the cluster with the nearest centroid (Euclidean distance)
5: Compute distances using Manhattan Distance for weight calculations
6: **end for**
7: **for all** clusters C_j **do**
8: Update centroid of C_j as the mean of all assigned points
9: **end for**
10: **until** convergence (no change in cluster assignments)=0

2) KDTREE FOR SPATIAL BLOCKING AND PROXIMITY SEARCH

KDTree [46], [47] is a binary space partitioning structure used for efficient multidimensional range and nearest-neighbor queries. In harness routing, a KDTree is constructed using the coordinates of restricted zones. Each candidate path node is queried against the KDTree to determine whether it falls within or near any restricted region, enabling fast, scalable spatial filtering.

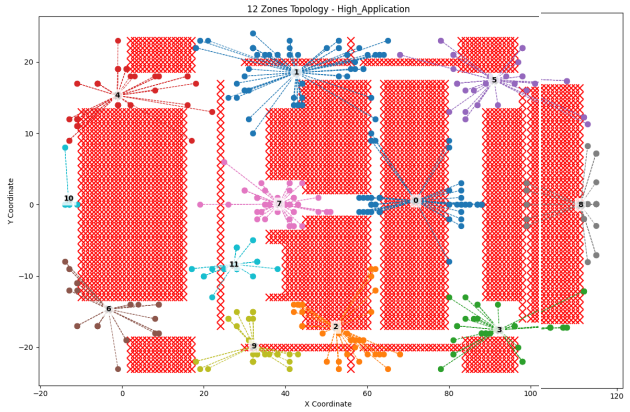

FIGURE 3. Clustered centroids and routing paths generated using Algorithm 1 without accounting for restricted zones (red zones). Routing paths and centroid placements are determined solely based on distance metrics, which may result in overlaps with physically invalid or blocked areas. Illustrated here is a 12-Zone topology for the high application tier.

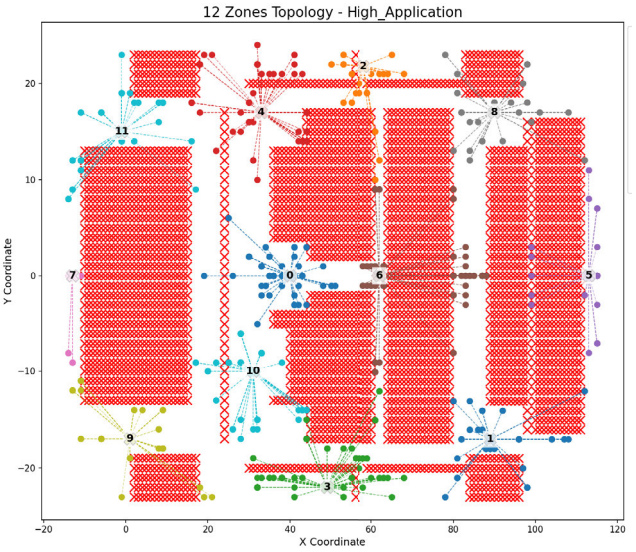

FIGURE 4. Improved centroid placement using Algorithm 1 combined with KDTree-based exclusion of restricted zones. In this configuration, centroids are repositioned to avoid restricted areas during initialization. For example, while in Fig. 3 the centroids of zones 0, 2, 8 and 9 fall within restricted regions, they are correctly placed outside these areas in the current figure. This reflects an optimized 12-Zone topology for the high application tier.

3) RESTRICTED ZONE-AWARE CENTROID PLACEMENT

To ensure that cluster centroids generated by K-means are spatially valid, the algorithm integrates a KDTree-based proximity check against restricted zones. After initial clustering, each centroid is examined for overlap or proximity to any restricted area. If a centroid falls within an unsafe distance, it is iteratively shifted in a normalized random direction until it lies outside the restricted region. This adjustment preserves spatial feasibility and prevents invalid routing origins. The corrected centroids are then clipped to dataset bounds and validated to avoid numerical instability, ensuring robust cluster assignments for harness routing optimization.

This refined centroid assignment supports physically realistic clustering outcomes, as illustrated in Fig. 4.

4) MANHATTAN DISTANCE FOR GRID-BASED ROUTING

In grid-based routing scenarios such as automotive wiring harness layouts, where movement is constrained to orthogonal (horizontal and vertical) directions, the Manhattan Distance is a widely used metric for estimating routing cost. It reflects the total number of horizontal and vertical steps required to traverse from a source point to a destination, assuming diagonal paths are not permitted.

Let $A = (x_1, y_1)$ and $B = (x_2, y_2)$ be two points on a 2D grid. The Manhattan Distance D_M is defined as:

$$D_M(A, B) = |x_2 - x_1| + |y_2 - y_1| \tag{2}$$

When scaled by a grid step size s (in millimeters), the physical wiring length L becomes:

$$L = s \cdot D_M(A, B) \tag{3}$$

5) BRESENHAM'S LINE ALGORITHM FOR PATH CLEARANCE

Bresenham's line algorithm is employed to determine a discrete linear path between two points in a rasterized grid, typically to validate line-of-sight or direct path clearance. The algorithm incrementally plots the nearest grid point to the ideal line at each step, ensuring minimal deviation from the intended trajectory. It is highly efficient and suitable for binary obstacle maps in routing contexts.

6) A* ALGORITHM FOR SHORTEST PATH SEARCH

The A* algorithm is employed to compute the shortest feasible path between two points in a grid while considering restricted zones and cost heuristics. At each iteration, it selects the node n that minimizes the cost function:

$$f(n) = g(n) + h(n) \tag{4}$$

where $g(n)$ is the actual cost from the start to node n, and $h(n)$ is the heuristic cost to the goal, typically computed using Manhattan Distance. A* ensures optimality and completeness under admissible heuristics.

Fig. 5 illustrates an example of all possible routing paths from the origin point $(0, 0)$ to a destination at $(6, 4)$, based on two types of movement: horizontal steps (denoted as M_1) and diagonal steps (M_2). In this context, M_1 refers to standard orthogonal grid traversal, while M_2 reflects potential diagonal approximations used in heuristic path planning.

Among these, the path computed by Bresenham's algorithm is shown using black arrows and represents the only valid line-drawing path that minimizes deviation from a straight trajectory between the start and end points. Alternative feasible paths, indicated by gray arrows, may still reach the target location while achieving the same vertical displacement but are less optimal for routing efficiency.

Restricted zones, which may obstruct direct travel, are identified using the A* search algorithm. When such obstacles are present, A* integrates obstacle-aware heuristics to guide Bresenham's algorithm toward a feasible, obstruction-free path. In scenarios where no obstacles exist between the source and destination, the Manhattan Distance is used as a fast, admissible estimate of path length, depicted as a dashed line in Fig. 5.

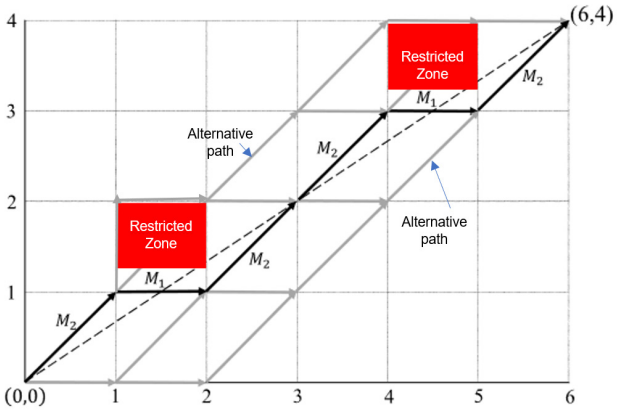

FIGURE 5. Example of all possible paths from the origin to the destination point using M1 (horizontal) and M2 (diagonal) movements.

7) DYNAMIC GRID ADAPTATION

Dynamic grid adaptation refers to modifying the resolution or size of the coordinate grid based on local component density or routing complexity. High-density zones use finer grids for accurate pathfinding, while sparse regions use coarser grids for computational efficiency. This enables a balance between routing precision and algorithmic scalability.

D. CLUSTERING EVALUATION METRICS

In K-means clustering, determining the optimal number of clusters k is critical to achieving meaningful and interpretable results. Several internal validation methods are proposed, such as the Calinski-Harabasz criterion, the Silhouette Coefficient, the gap statistic, the Davies-Bouldin index, and cluster ensemble techniques. In this work, we adopt four commonly used metrics—namely the Silhouette Coefficient, the Calinski-Harabasz criterion, the Elbow method, and the Davies-Bouldin index—to evaluate clustering performance across a range of cluster sizes.

The Silhouette Coefficient quantifies the compactness and separation of clusters. For each sample q, the silhouette score $s(q)$ is defined as:

$$s(q) = \frac{b(q) - a(q)}{\max\{a(q), b(q)\}}, \quad q = 1, 2, \ldots, n \tag{5}$$

where $a(q)$ is the average intra-cluster distance (i.e., the average distance from point q to all other points in the same cluster), and $b(q)$ is the minimum average distance from point q to points in a different cluster. The silhouette score ranges from -1 to 1, with higher values indicating better clustering.

The Calinski-Harabasz index evaluates the ratio between inter-cluster and intra-cluster dispersion:

$$C_k = \frac{\text{SSB}}{\text{SSW}} \cdot \frac{n-k}{k-1} \tag{6}$$

where SSB and SSW represent the between-cluster and within-cluster sum of squares, respectively, n is the number of samples, and k is the number of clusters. Higher values of C_k indicate better-defined clusters.

The Elbow method relies on plotting the within-cluster sum of squares (WCSS) against various values of k. The optimal number of clusters is typically located at the ''elbow'' point in the curve, where adding more clusters yields diminishing returns in reducing WCSS.

The Davies-Bouldin index measures the average similarity between each cluster and its most similar counterpart. It is defined as:

$$DB = \frac{1}{k}\sum_{i=1}^{k} \max_{j \neq i} \left(\frac{s_i + s_j}{d_{ij}} \right) \tag{7}$$

where s_i and s_j are the average distances of points within clusters i and j to their respective centroids, and d_{ij} is the Euclidean distance between centroids i and j. Lower values of the Davies-Bouldin index indicate better clustering quality.

These four methods were applied simultaneously across a range of k values (typically $k = 1$ to 16), and visualized together for comparative interpretation. This multi-metric approach provides a more robust and interpretable estimate of the optimal number of clusters across Low, Mid, and High application wiring harness scenarios.

Fig. 6 summarizes the evaluation metrics for determining the optimal number of clusters in the High Application scenario. The dataset was standardized and analyzed with k ranging from 1 to 16. The Elbow method (Fig. 6(a)) suggests $k = 8$ as a turning point. The Calinski-Harabasz criterion in Fig. 6(b) peaks at $k = 16$, while Silhouette and Davies-Bouldin scores indicate optimal performance at $k = 9$ and $k = 12$. However, Fig. 6(c) shows negative Silhouette Coefficients for $k = 9$ and $k = 13$, whereas $k = 8$ and $k = 12$ yield better clustering separation. Thus, $k = 12$ is recommended for its stability across all criteria.

Fig. 7 presents the clustering quality metrics for the Mid Application dataset. The Elbow method in Fig. 7(a) shows that $k = 6$ may serve as a knee point. As seen in Fig. 7(b), the Calinski-Harabasz index reaches its highest at $k = 14$, and both Silhouette and Davies-Bouldin scores perform best for $k = 9$ through $k = 14$. From Fig. 7(c), $k = 10$ and $k = 14$ produce stable, high Silhouette Coefficients, while $k = 8$, $k = 9$, and $k = 13$ demonstrate signs of clustering instability. Therefore, $k = 14$ is preferred for its overall performance and cohesion.

Fig. 8 illustrates clustering evaluation metrics for the Low Application case, tested for $k = 1$ to $k = 12$. In Fig. 8(a), $k = 6$ is a candidate based on the Elbow method. Fig. 8(b) reveals maximum Calinski score at $k = 12$ and peak Silhouette and Davies-Bouldin scores near $k = 11$ and $k = 12$. Fig. 8(c) indicates that $k = 11$ yields the most consistent and positive silhouette distribution, while $k = 6$, $k = 10$, and $k = 12$ show mixed or negative results. Hence, $k = 11$ is identified as the optimal clustering configuration for this application type.

IV. RESULTS AND DISCUSSION

A. ANALYSIS OF 12-ZONAL CLUSTER CONFIGURATION FOR HIGH APPLICATION

Overall, these findings validate the clustering outcomes obtained from the evaluation metrics (Figs. 6–8), and substantiate the technical rationale for selecting $k = 12$ clusters in the high application scenario. This configuration is thus selected for detailed analysis in the subsequent section, which examines component-level routing, domain-wise mapping, and the alignment between real and synthetic layout structures.

TABLE 3. Detailed statistics for Cluster 12 (High Application) showing zone-wise metrics.

Zone ID	Components	Pinout Density	Distance (m)	Weight (g)
0	48	133	8.496	114.26
1	52	179	28.620	527.10
2	20	44	5.508	70.14
3	18	66	6.948	134.47
4	63	148	33.228	622.29
5	19	54	3.384	56.57
6	64	146	28.692	323.39
7	15	60	4.068	132.57
8	35	97	14.364	254.43
9	19	54	8.172	275.08
10	44	135	21.744	311.06
11	20	72	6.840	146.43

1) CLUSTER-LEVEL ROUTING AND DOMAIN SYNTHESIS

Table 3 presents zone-level statistics for Cluster 12 in the high application routing scenario. The table includes component counts, pinout densities, total routed distance, and cumulative wiring weight per zone. Notably, zones 1, 4, and 6 exhibit the highest weight and distance values due to higher component loads and longer internal routing paths. By contrast, zones 2 and 5 are more compact and localized. This insight demonstrates the cluster's capacity to accommodate varied spatial demands while maintaining design balance.

2) COMPONENT-LEVEL ROUTING UNDER RESTRICTED-ZONE-AWARE CLUSTERING

Table 4 presents sample routing and weight computations for a 12-Zone configuration under the high application scenario. Clustering is performed using the K-means algorithm based on the shortest Euclidean distance, as described in Algorithm 1. Routing paths are then computed using the Dynamic Grid, Manhattan Distance, A*, and Bresenham's algorithms, as detailed in Algorithm 2 and illustrated in Fig. 5.

For example, component Index 796 is initially associated with Centroid (40.00, 0.00) under Cluster ID 0. Following routing using A* and Bresenham's methods within a dynamic grid system, the centroid is reassigned to (33.00, 17.00) under

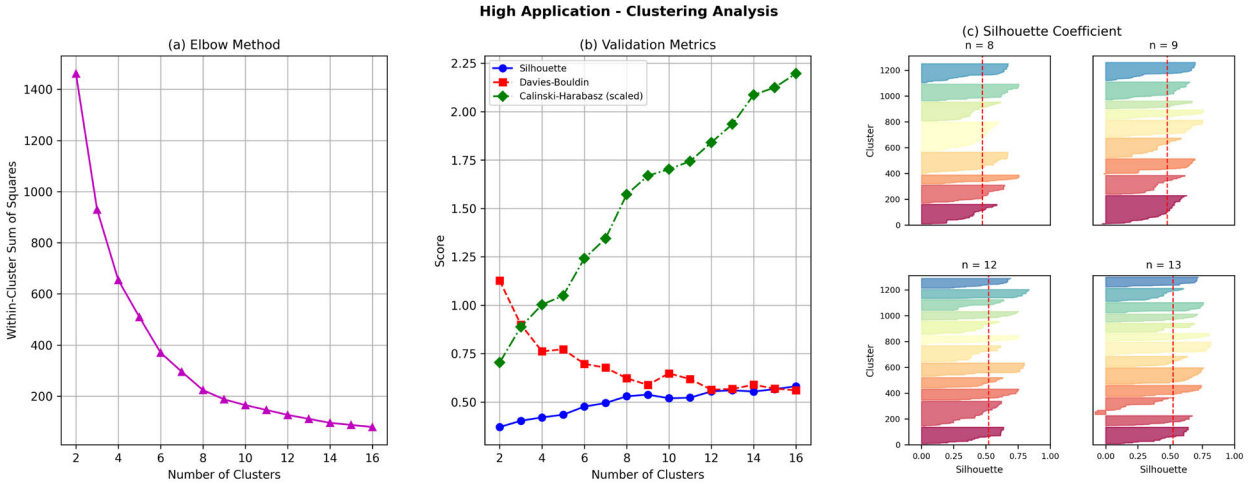

FIGURE 6. Cluster selection criteria for determining the optimal number of K-means clusters for the high application scenario. (a) Elbow method. (b) Silhouette score, Davies–Bouldin index, and Calinski–Harabasz criterion. (c) Silhouette Coefficient distribution. Based on these evaluation metrics, $k = 12$ is selected as the optimal number of clusters for this application.

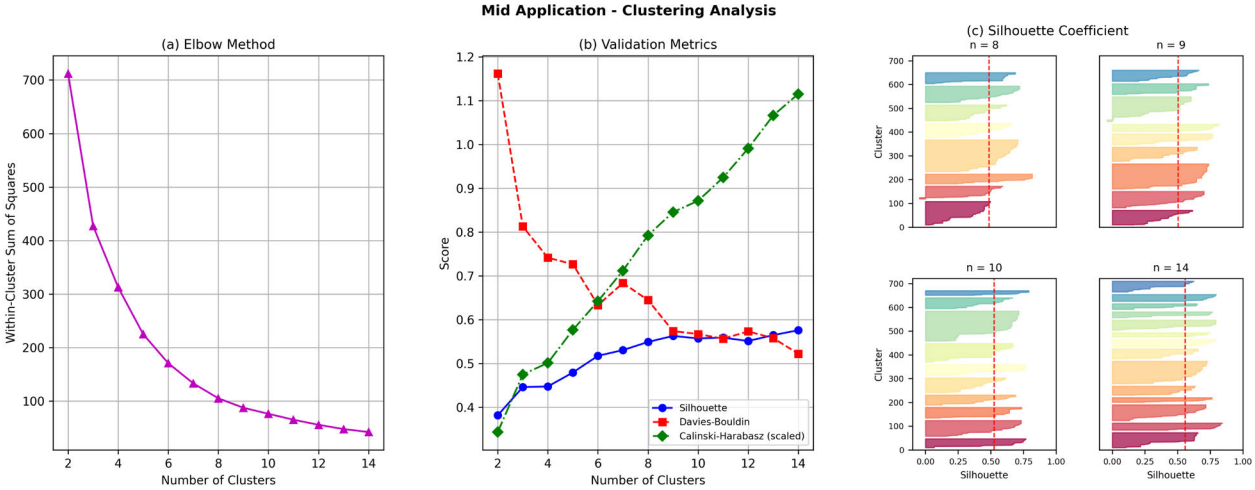

FIGURE 7. Cluster selection criteria for determining the optimal number of K-means clusters for the mid application scenario. (a) Elbow method. (b) Silhouette score, Davies–Bouldin index, and Calinski–Harabasz criterion. (c) Silhouette Coefficient distribution. Based on these evaluation metrics, $k = 14$ is selected as the optimal number of clusters for this application.

TABLE 4. Sample component routing and weight computation for 12-Zone high application using K-means clustering, Dynamic Grid, Manhattan Distance, A*, and Bresenham's algorithms.

Index	Index Coord	Centroid	Routed Centroid	Cluster ID	Wire Wt. (g/m)	Start Grid	Target Grid	Path Type	Dir Steps	A* Steps	Used Steps	Distance (m)	Index Wt. (g)
1	35.00;0.00	40.00;0.00	40.00;0.00	0	67.5	(49,25)	(54,25)	Direct	5	-	5	0.180	12.15
8	36.00;0.00	40.00;0.00	40.00;0.00	0	19.12	(50,25)	(54,25)	Direct	4	-	4	0.144	2.75
9	36.00;0.00	40.00;0.00	40.00;0.00	0	19.12	(50,25)	(54,25)	Direct	4	-	4	0.144	2.75
111	33.00;-2.00	40.00;0.00	40.00;0.00	0	4.08	(47,23)	(54,25)	Direct	9	-	9	0.324	1.32
175	33.00;1.00	40.00;0.00	40.00;0.00	0	46.6	(47,26)	(54,25)	Direct	8	-	8	0.288	13.42
356	43.00;0.00	40.00;0.00	40.00;0.00	0	10.02	(57,25)	(54,25)	Direct	3	-	3	0.108	1.08
795	33.00;-1.00	40.00;0.00	40.00;0.00	0	4.08	(47,24)	(54,24)	Direct	8	-	8	0.288	1.18
796	19.00;0.00	40.00;0.00	33.00;17.00	4	20.07	(33,25)	(47,42)	A*	31	33	33	1.188	23.84
4097	32.00;-5.00	40.00;0.00	31.00;-10.00	10	12.64	(46,20)	(45,15)	Direct	6	-	6	0.216	2.73
10031	25.00;6.00	40.00;0.00	33.00;17.00	4	255.52	(39,31)	(47,42)	Direct	19	-	19	0.684	174.78
4016	107.00;-17.00	89.00;-17.00	89.00;-17.00	1	8.16	(121,8)	(103,8)	Direct	18	-	18	0.648	5.29
4141	112.00;-12.00	89.00;-17.00	113.00;0.00	5	16.5	(126,13)	(127,25)	Direct	13	-	13	0.468	7.72
4318	78.00;-23.00	89.00;-17.00	62.00;0.00	6	12.78	(92,2)	(76,25)	A*	-	47	47	1.692	21.62
5355	81.00;21.00	89.00;-17.00	62.00;0.00	6	33.78	(95,4)	(76,25)	A*	-	48	48	1.728	58.37
6211	96.00;-17.00	89.00;-17.00	89.00;-17.00	1	4.08	(110,8)	(103,8)	Direct	7	-	7	0.252	1.03
7053	80.00;-13.00	89.00;-17.00	89.00;-17.00	1	8.52	(94,12)	(103,8)	Direct	13	-	13	0.468	3.99
7057	98.00;-22.00	89.00;-17.00	89.00;-17.00	1	4.26	(112,3)	(103,8)	A*	-	14	14	0.504	2.15
9058	96.00;-17.00	89.00;-17.00	89.00;-17.00	1	135.64	(110,8)	(103,8)	Direct	7	-	7	0.252	34.18
9169	98.00;-22.00	89.00;-17.00	89.00;-17.00	1	36.78	(112,3)	(103,8)	A*	-	14	14	0.504	18.54
9183	82.00;-17.00	89.00;-17.00	89.00;-17.00	1	225.34	(96,8)	(103,8)	Direct	7	-	7	0.252	56.79

Cluster ID 4. The presence of restricted zones increases the path length, requiring 33 A* steps despite only 31 direct grid steps. Grid coordinates are obtained by discretizing the vehicle coordinate space, where each unit represents 36 mm.

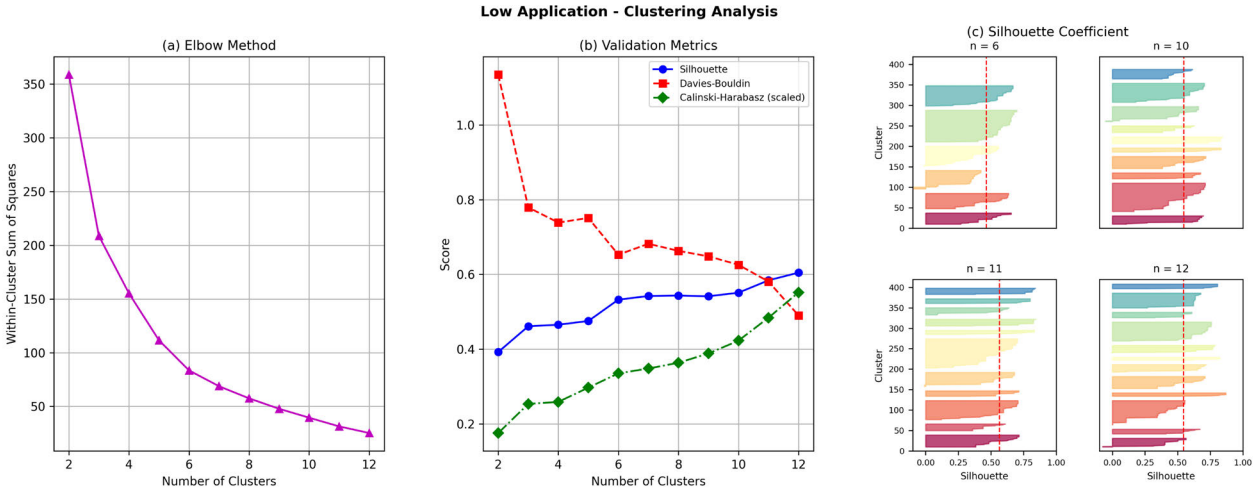

FIGURE 8. Cluster selection criteria for determining the optimal number of K-means clusters for the low application scenario. (a) Elbow method. (b) Silhouette score, Davies–Bouldin index, and Calinski–Harabasz criterion. (c) Silhouette Coefficient distribution. Based on these evaluation metrics, $k = 11$ is selected as the optimal number of clusters for this application.

Algorithm 2 RoutingPathOptimization(Grid, Source, Target, R)

Input: Grid of coordinate cells, source point, target point, and restricted cells R

Output: Feasible path P and distance d

Initialize open list with Source node
Set all grid cells as unvisited
Apply spatial mask to mark restricted zones in R as blocked
While open list is not empty **do**
  Select node n with lowest cost: $f(n) = g(n) + h(n)$
  if n is the Target **then**
    Reconstruct path P by backtracking from n
    Compute total distance d (e.g., Manhattan)
    return P, d
  end if
  Mark n as visited
  for all valid neighbors n' of n **do**
    if n' is blocked or visited **then**
      continue
    end if
    Update cost $g(n') = g(n) + \texttt{step\_size}$
    Estimate $h(n')$ using Manhattan Distance
    Add n' to open list with priority $f(n')$
  end for
end while
return no path found=0

Thus, the total routing distance is 33×0.036 m $= 1.188$ m, and the corresponding wire weight is calculated as 1.188 m $\times\ 20.07 g/m = 23.84$ g.

Similarly, Index 4097 is initially linked to Centroid (40.00, 0.00) and reassigned to (31.00, −10.00) under Cluster ID 10. Since the path does not intersect restricted zones, a direct Manhattan route is applied, resulting in 6 steps and a total distance of $6 \times 0.036 = 0.216$ m. With a wire gauge weight of 12.64 g/m, the resulting connection weight is 0.216 m $\times$ 12.64 g/m $= 2.73$ g.

These case studies demonstrate how restricted-zone-aware routing impacts centroid reassignment, routing complexity, and wire mass across zonal configurations.

3) INTER-CENTROID WIRING STRATEGY FOR RING TOPOLOGY FORMATION

Table 5 presents the Centroids-to-Centroids interconnection routes designed using a ring topology for data communication, a widely adopted method for enhancing network redundancy and fault tolerance in distributed automotive systems. This structure ensures that, even in the event of a node failure, alternate communication paths remain available. The routing metrics—such as physical distance (in meters), grid step count, and associated wire weight (in grams)—are crucial for evaluating both spatial feasibility and economic impact.

To construct the ring, centroid pairs are sorted by proximity, and each centroid is limited to a maximum of two connections. This constraint enforces a minimally connected, yet loop-capable topology. For each eligible pair, the A* pathfinding and Bresenham's algorithms—described in Algorithm 2 and visualized in Fig. 5—are used to compute feasible routes while avoiding restricted vehicle zones. Step counts are converted into physical distance using a fixed grid-to-meter scale. Total wiring mass is then calculated by multiplying the path length with a standard wire weight coefficient, derived from lightweight twisted-pair communication cables (e.g., FLRY 2×0.35 at 4.26 g/m), as defined in Table 2.

TABLE 5. Centroids-to-Centroids routing details of 12 zonal cluster high application for Inter-Zone communication (Ring Topology).

Src Clust.	Dst Clust.	Src Coord	Dst Coord	Src Grid	Dst Grid	Conn. Type	Grid Dist.	Steps	Distance (m)	Weight (g)
0	10	40.00;0.00	31.00;-10.00	54;25	45;15	$0 \leftrightarrow 10$	19	19	0.684	2.91
0	4	40.00;0.00	33.00;17.00	54;25	47;42	$0 \leftrightarrow 4$	24	24	0.864	3.68
7	11	-13.00;0.00	-1.00;15.00	1;25	13;40	$7 \leftrightarrow 11$	27	27	0.972	4.14
3	10	49.00;-22.00	31.00;-10.00	63;3	45;15	$3 \leftrightarrow 10$	30	34	1.224	5.21
7	9	-13.00;0.00	1.00;-17.00	1;25	15;8	$7 \leftrightarrow 9$	31	31	1.116	4.75
2	6	58.11;21.79	62.00;0.00	72;47	76;25	$2 \leftrightarrow 6$	26	26	0.936	3.99
2	4	58.11;21.79	33.00;17.00	72;47	47;42	$2 \leftrightarrow 4$	30	30	1.080	4.60
3	6	49.00;-22.00	62.00;0.00	63;3	76;25	$3 \leftrightarrow 6$	35	75	2.700	11.50
5	8	113.00;0.00	90.00;17.00	127;25	104;42	$5 \leftrightarrow 8$	40	40	1.440	6.13
1	5	89.00;-17.00	113.00;0.00	103;8	127;25	$1 \leftrightarrow 5$	41	41	1.476	6.29
9	11	1.00;-17.00	-1.00;15.00	15;8	13;40	$9 \leftrightarrow 11$	34	54	1.944	8.28
1	8	89.00;-17.00	90.00;17.00	103;8	104;42	$1 \leftrightarrow 8$	35	37	1.332	5.67

The resulting centroid interconnections for the 12-Zone high application scenario show path lengths ranging from 0.684 m to 2.7 m and corresponding wire weights from 2.91 g to 11.50 g. Notably, connections such as Cluster $9 \leftrightarrow 11$ yield higher wire mass due to extended routing paths, highlighting critical inter-zone links that may demand shielding or bandwidth prioritization in domains like ADAS or infotainment.

By quantifying these metrics, the strategy allows designers to balance robust communication with lightweight and scalable design principles—essential for electric and autonomous vehicles, where minimizing wiring complexity translates into gains in energy efficiency, serviceability, and cost.

4) CENTROIDS-TO-BATTERY CONNECTION STRATEGY BASED ON CLUSTER CURRENT DEMAND

To ensure proper power delivery in zonal electronic architectures, a current-aware routing framework is employed to determine optimal wire types and compute total wiring mass between each cluster centroid and the central battery. For every zone, the total current requirement is computed by aggregating the nominal power consumption of all components within the cluster and converting it to current using the relation $I = P/12$ V, assuming a standardized 12 V supply.

The computed current demand per cluster is then compared against standard automotive wire types, each characterized by a rated current-carrying capacity and weight per unit length, as listed in Table 2. The lightest wire capable of safely carrying the cluster's required current is selected as the battery wire type. This ensures adherence to ISO-standardized electrical safety and performance guidelines while minimizing cable weight.

The Centroids-to-Battery routing is computed using a restricted-zone-aware A* pathfinding and Bresenham's algorithms (Algorithm 2 and illustrated in Fig. 5), which ensures that cable paths avoid physical and regulatory constraints in the vehicle geometry. grid-based distances between centroids and the fixed battery location (98.0, 18.0) are translated to meters using a calibrated scale (e.g., 36 mm per grid unit), and the resulting lengths are multiplied by the corresponding wire mass to calculate the total connection weight for each zone.

Algorithm 3 Harness Optimization With Cluster-Level Current Estimation and Battery Connection Weighting

Input: Component dataset D, Wire characteristics table W, Cluster sizes S, Battery location B, Voltage $V = 12$ V

Output: Cluster assignments, total Centroids-to-Battery wire weight, and distance per application scenario

Extract nominal power $P_{nominal}$ and coordinates from D
Compute nominal current for each component: $I = P_{nominal}/V$
Apply preprocessing to filter connected components (PowerSupply = Yes and Signal = No)
Convert coordinates to grid and remove restricted-zone overlaps
for all cluster size $k \in S$ **do**
    Apply KMeans clustering with k clusters
    Assign each component to its nearest cluster centroid
    for all cluster ID c **do**
        Sum nominal current: $I_c = \sum I_{component \in c}$
        From W, find wire type where capacity $\geq I_c$
        Retrieve corresponding wire weight w_c [g/m]
        Routed path from centroid c to Battery B using routing (see Alg. 2)
        Compute distance d_c and weight $W_c = d_c \times w_c$
    end for
    Save total weight $\sum_c W_c$ and routing summary for k
end for
return configuration with minimum total weight for each application (Low, Mid, High)=0

As shown in Table 6, clusters with higher current demands—such as Cluster 1 and Cluster 4—require high-capacity wires (e.g., FLY 120.00) and result in heavier battery connection weights (e.g., 2053.44 g and 2946.24 g, respectively). In contrast, clusters with moderate demands (e.g., Cluster 0 or Cluster 2) utilize lighter wire types and incur lower routing overhead.

This connection logic, formalized in Algorithm 3, ensures electrical feasibility while optimizing for total harness weight, a critical factor in electric vehicle design. By

TABLE 6. Centroids-to-Battery connection based on centroid-demanded nominal current matched with wire current-carrying capacity, used to determine optimal battery wire type and compute total battery connection wire weight for 12-Zone high application.

Cluster ID	Required Current (A)	Wire Capacity (A)	Battery Wire Type	Wire Weight (g/m)	Source Coord.	Dest. Coord.	Source Grid	Dest. Grid	Steps	Distance (m)	Battery Weight (g)
0	42.86	42.88	FLRY 6.00	58.71	40.00;0.00	98.0;18.0	54;25	112;43	76	2.736	160.63
1	279.37	279.56	FLY 120.00	1240.00	89.00;-17.00	98.0;18.0	103;8	112;43	46	1.656	2053.44
2	36.15	37.64	FLRY 5.00	50.00	58.11;21.79	98.0;18.0	72;47	112;43	44	1.584	79.20
3	69.22	70.27	FLRY 12.00	127.00	49.00;-22.00	98.0;18.0	63;3	112;43	129	4.644	589.79
4	276.39	279.56	FLY 120.00	1240.00	33.00;17.00	98.0;18.0	47;42	112;43	66	2.376	2946.24
5	99.75	110.10	FLRY 25.00	247.00	113.00;0.00	98.0;18.0	127;25	112;43	33	1.188	293.44
6	177.27	184.40	FLRY 60.00	592.00	62.00;0.00	98.0;18.0	76;25	112;43	54	1.944	1150.85
7	202.58	206.16	FLRY 70.00	702.00	-13.00;0.00	98.0;18.0	1;25	112;43	129	4.644	3260.09
8	262.60	279.56	FLY 120.00	1240.00	90.00;17.00	98.0;18.0	104;42	112;43	9	0.324	401.76
9	216.01	227.39	FLRY 85.00	761.60	1.00;-17.00	98.0;18.0	15;8	112;43	132	4.752	3619.12
10	197.03	206.16	FLRY 70.00	702.00	31.00;-10.00	98.0;18.0	45;15	112;43	95	3.420	2400.84
11	217.31	227.39	FLRY 85.00	761.60	-1.00;15.00	98.0;18.0	13;40	112;43	102	3.672	2796.60

integrating nominal current estimation, wire selection, and path-based routing, this method enables scalable, safety-compliant, and lightweight harness planning across Low, Mid, and High application tiers.

5) HIGH-PERFORMANCE COMPUTER (HPC) POSITIONING AND ROUTING STRATEGY

To minimize interconnect overhead and enhance processing centrality, the HPC position is determined using a medoid-based selection method. Candidate grid positions—filtered to exclude any overlap with restricted zones—are evaluated based on their total Manhattan (cityblock) distance to all valid cluster centroids. The grid point with the minimum cumulative distance is selected as the optimal HPC location, thereby reducing the total wire length between zone controllers and the central unit.

After determining the HPC location, optimal routing paths are generated using A* search and Bresenham's line algorithms, as detailed in Algorithm 2 and illustrated in Fig. 5. The number of routing steps is translated into meters using a fixed grid resolution, and wire mass is computed by multiplying path length by a standardized Ethernet cable weight (e.g., FLKS9Y 2×0.13, 6.0 g/m) as defined in Table 7. This cable type supports 100 Mbit/s, making it appropriate for inter-zone backbone communication.

Table 8 consolidates routing metrics across all twelve clusters under the high application scenario. Each row details the domain composition, internal Components-to-Centroids distances, inter-centroid (ring topology) links, Centroids-to-HPC connections, and Centroids-to-Battery power paths. Notably, clusters 1, 4, and 6 exhibit higher total wire weight due to their functional density and roles in core domains such as Drive Assistance, Powertrain, and Chassis. In contrast, clusters 2 and 5 show reduced wiring requirements, reflecting simpler and more localized subsystems.

This comprehensive routing analysis enables evaluation of system modularity, data backbone efficiency, and power distribution overhead, supporting harness design optimization for electric and autonomous vehicles.

6) DOMAIN-LEVEL ANALYSIS OF ZONAL CLUSTER DISTRIBUTION

Fig. 9 presents the domain-wise distribution of clusters in the High Application scenario. Each cluster is mapped to functional domains such as Comfort, Chassis, Infotainment, and others, based on its constituent components.

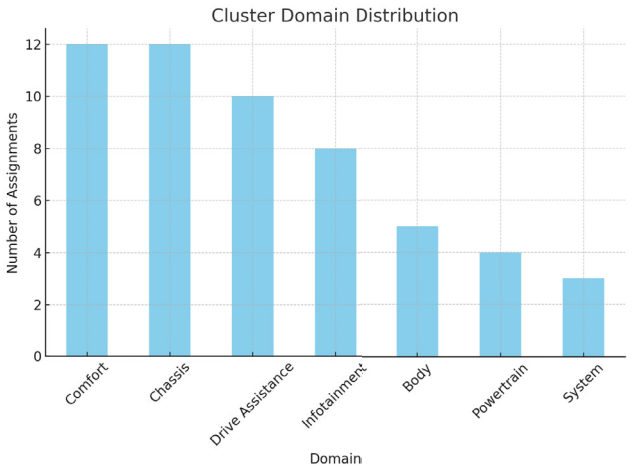

FIGURE 9. Domain-wise distribution of clusters in the high application scenario.

The Comfort and Chassis domains exhibit the highest frequency, each appearing in 12 cluster assignments, indicating a dominant share of user-centric and vehicular control functions. Drive Assistance and Infotainment follow with 10 and 8 assignments, respectively, reflecting the system's support for ADAS and multimedia services.

Conversely, domains like Powertrain (4), System (3), and Body (5) appear less frequently, suggesting centralized or function-specific placement in high-load designs. These insights are critical for optimizing inter-domain communication links, ensuring balanced resource allocation, and guiding domain-aware harness partitioning in zonal E/E architectures.

7) AI-GENERATED VERSUS MANUAL HARNESS DESIGN

Fig. 10 compares the AI-based harness routing result with the manual design used by KI4BoardNet project partners EDAG and KROSCHU. The top part illustrates the automated layout for the 12-cluster high application scenario. This includes Components-to-Centroids wiring, Centroids-to-HPC and battery links, and inter-centroid communication, all avoiding restricted zones (white areas). Components are spatially grouped into 12-Zone (IDs 0–11), and the A*-based routing ensures compliance with spatial constraints.

The bottom figure shows the traditional manual layout, in which restricted areas (red zones) and component locations

TABLE 7. Centroids-to-HPC connection based on a fixed FLKS9Y 2 × 0.13 Ethernet wire, rated at 6 g/m and supporting 100 Mbit/s data transmission. The path type, Manhattan and actual steps are used to compute the total connection distance and corresponding HPC wire weight for each cluster, as well as the total Centroids-to-HPC connection wire weight for the 12-Zone high application.

Cluster ID	Centroid Coord.	HPC Position	Start Grid	Target Grid	Path Type	Manhattan Steps	Actual Steps	Used Steps	Distance (m)	Centroid-HPC Weight (g)
0	40.00;0.00	54;25	54;25	54;25	Direct	0	0	0	0.000	0.00
1	89.00;-17.00	54;25	103;8	54;25	A*	66	68	68	2.448	14.69
2	58.11;21.79	54;25	72;47	54;25	A*	40	46	46	1.656	9.94
3	49.00;-22.00	54;25	63;3	54;25	A*	31	53	53	1.908	11.45
4	33.00;17.00	54;25	47;42	54;25	A*	24	24	24	0.864	5.18
5	113.00;0.00	54;25	127;25	54;25	A*	73	109	109	3.924	23.54
6	62.00;0.00	54;25	76;25	54;25	Direct	22	22	22	0.792	4.75
7	-13.00;0.00	54;25	1;25	54;25	A*	53	89	89	3.204	19.22
8	90.00;17.00	54;25	104;42	54;25	A*	67	69	69	2.484	14.90
9	1.00;-17.00	54;25	15;8	54;25	A*	56	58	58	2.088	12.53
10	31.00;-10.00	54;25	45;15	54;25	A*	19	19	19	0.684	4.10
11	-1.00;15.00	54;25	13;40	54;25	A*	56	62	62	2.232	13.39

TABLE 8. Cluster-wise breakdown of routing distance and weight for components-to-centroid, inter-centroid, Centroids-to-HPC, and Centroids-to-Battery connections, along with associated domain roles in the 12-Zone high application configuration.

Cluster ID	Domain	Components-Centroid		Centroid-Centroid		Centroid-HPC		Centroid-Battery		Total	
		Dist. (m)	Weight (g)	Dist. (m)	Weight (g)	Dist. (m)	Weight (g)	Dist. (m)	Weight (g)	Dist. (m)	Weight (g)
0	Infotainment	8.496	114.26	0.684	2.91	0	0	2.736	160.63	11.916	277.80
1	Chassis / Powertrain / Comfort / Infotainment / Drive Assist / Body	28.62	527.10	0.864	3.68	2.448	14.69	1.656	2053.44	33.588	2598.91
2	Comfort / Chassis / Infotainment	5.508	70.14	0.972	4.14	1.656	9.94	1.584	79.2	9.720	163.42
3	Comfort / Chassis / Infotainment	6.948	134.47	1.224	5.21	1.908	11.45	4.644	589.79	14.724	740.92
4	Comfort / Chassis / Drive Assist / Infotainment / Powertrain	33.228	622.29	1.116	4.75	0.864	5.18	2.376	2946.24	37.584	3578.46
5	Comfort / Chassis / Drive Assist	3.384	56.57	0.936	3.99	3.924	23.54	1.188	293.44	9.432	377.54
6	Comfort / Chassis / Infotainment / Drive Assist / Body	28.692	323.39	1.080	4.60	0.792	4.75	1.944	1150.85	32.508	1483.59
7	Comfort / Chassis / Drive Assist / System	4.068	132.57	2.700	11.50	3.204	19.22	4.644	3260.09	14.616	3423.38
8	Comfort / Infotainment / System / Drive Assist / Body	14.364	254.43	1.440	6.13	2.484	14.9	0.324	401.76	18.612	677.22
9	Chassis / Comfort / Drive Assist	8.172	275.08	1.476	6.29	2.088	12.53	4.752	3619.12	16.488	3913.02
10	Comfort / Powertrain / Drive Assist / Infotainment / System	21.744	311.06	1.944	8.28	0.684	4.1	3.420	2400.84	27.792	2724.28
11	Chassis / Drive Assist / Comfort / Body	6.840	146.43	1.332	5.67	2.232	13.39	3.672	2796.60	14.076	2962.09
Total	—	170.064	2967.79	15.768	67.17	22.284	133.69	32.94	19752	241.056	22,920.65

(marked by crosses) are identified, but wiring is not fully implemented due to the high time and cost involved in manual design. Unlike the AI-generated version, which completes full routing and zone-wise optimization, the manual design lacks feasible automated routing. The visual alignment demonstrates that the AI method not only replicates but enhances layout clarity and harness feasibility for real-world implementation.

B. SCALABILITY ANALYSIS OF MULTI-ZONAL CLUSTER CONFIGURATIONS ACROSS VEHICLE APPLICATION CLASSES

To evaluate the scalability of the harness architecture beyond the validated 12-zonal cluster, the same methodology—including clustering, domain synthesis, restricted-zone-aware routing, and Components-to-Centroids, inter-centroid, HPC, and battery connections—is extended to zonal configurations ranging from 1 to 14 clusters. Table 9 and Table 10 summarize the total routing distances (in meters) and corresponding wiring weights (in grams) for three routing scopes (component paths, data communication, and power supply) across Low, Mid, and High application variants.

The results reveal that while decreased zonal granularity (e.g., 10–14 clusters) offers modularity and improved spatial distribution, it also leads to a rise in total wiring weight—particularly for power supply paths. For example, the 12-Zone high application requires a total of 241.056 m and 22,920.65 g of wiring, whereas the 11-Zone configuration shows comparable distance (254.844 m) but slightly higher weight (23,980.03 g), indicating a trade-off between functional partitioning and wiring mass. In contrast, minimal configurations (e.g., 1–3 clusters) suffer from excessive interconnect distance due to limited spatial distribution, thereby highlighting the design-space sweet spot achieved at 12 zones for high application. These findings support the scalability of the proposed clustering and routing framework while guiding optimal cluster count selection for diverse vehicle applications.

C. COMPARISON WITH EXISTING METHODS

To evaluate the effectiveness of the proposed AI-based zonal clustering and routing approach, we compared our results with existing methods reported in the literature. Table 11 summarizes key benchmarks for wiring length and weight across different numbers of ECUs and architectural strategies.

Park et al. [32] reported a total wiring length of approximately 100 m and a weight of 3.9 kg for a 10-Zone ZIA with 120 ECUs in a vehicle measuring 4.8 m in length and 2 m in width. In contrast, Stillig and Parspour [48] highlighted that traditional harness designs can reach up to 1.6 km and 60 kg in large vehicles. Park and Park [31] further compared domain-based IVN (DIA) and zone-based IVN (ZIA) architectures for 60 ECUs, showing that ZIA reduced wiring length from 65.05 m to 49.02 m and weight from 2.44 kg to 1.84 kg. Finally, Lee [49] noted that conventional designs with approximately 150 ECUs could require up to 5 km of wiring.

In our approach, for a vehicle measuring 4.76 m in length and 1.85 m in width, we achieve superior scalability as the number of ECUs increases. For the 12-Zone high application scenario with 417 ECUs, the proposed method achieves a total wiring length of 241.056 m and a total weight of 22.92 kg. For the mid and low application scenarios with 206 and 103 ECUs, wiring lengths of 147.528 m and 113.4 m, and corresponding weights of 7.53 kg and 3.87 kg, respectively, were obtained. Compared

(a) Manually prepared layout

(b) AI-based harness design

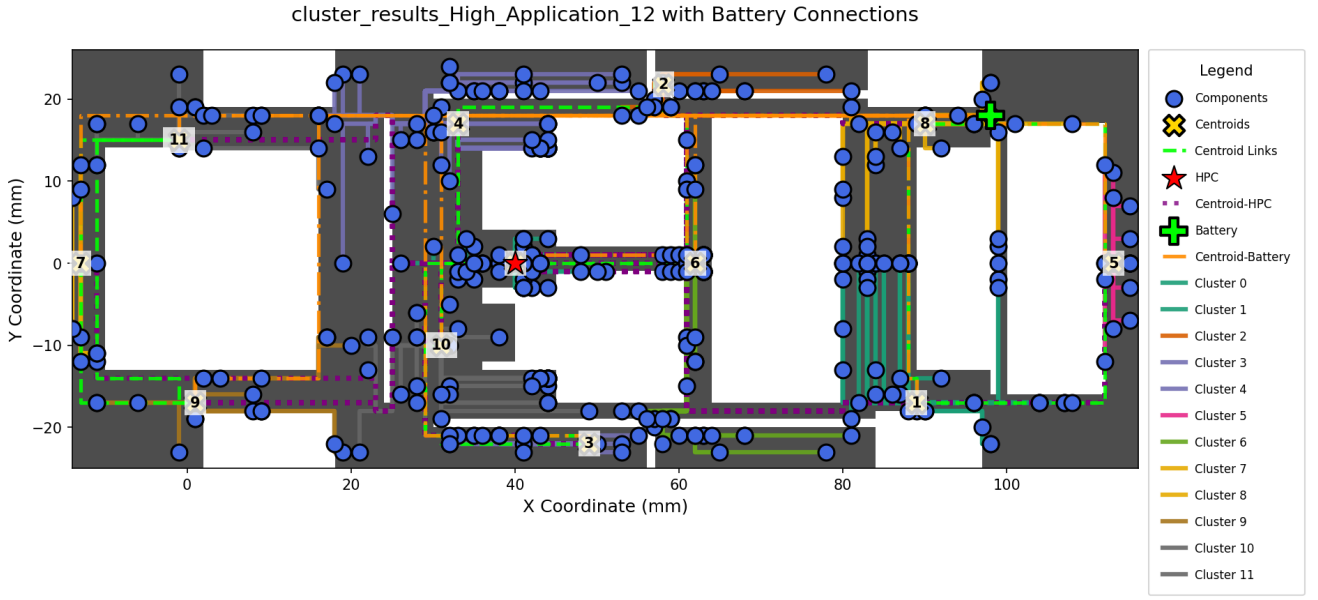

FIGURE 10. Comparison of layout inputs and AI-based harness design for the 12-Zone high application scenario.(a) Manually prepared layout created by project partners (EDAG, KORSCHU) using spreadsheets, showing component positions and restricted zones (in red), without routing paths.(b) AI-based harness design with full routing, automatically generated using K-means clustering, A*, Bresenham's algorithm, Manhattan Distance, and grid search—avoiding restricted areas while reducing design time, cost, and weight.

to prior studies, the proposed method significantly reduces wiring length and weight even as the number of ECUs increases beyond the levels considered in earlier work. This highlights the efficiency of the AI-driven zonal clustering and routing algorithms in handling high-complexity, large-scale designs.

It is important to note that the wiring weight in the 12-Zone high application scenario is higher (22.92 kg) than some prior studies, such as Park et al. [32], which reported 3.9 kg for 120 ECUs. This difference arises because the present methodology accounts for realistic factors often overlooked in earlier work. Specifically, multiple wire types are used for both power and data communication, including FLRY95.00 with a weight of 911.00 g/m for power connections, and FLKS9Y2 × 0.13 Ethernet cable rated at 100 Mbit/s with a weight of 6 g/m for data communication, whereas Park et al. [32] assumed a uniform harness weight of 0.0375 kg/m.

TABLE 9. Comparison of clustering total distance results (in m) across selected routing strategies and application scenarios. The distance for data communication is computed as the sum of Centroids-to-Centroids and Centroids-to-HPC paths, while the power supply distance is computed from Centroids-to-battery paths. The total distance combines the components path (avoiding restricted zones), data communication, and power supply according to the application scenario.

Zonal	ComponentsPathAvoidRZ			ForDataCommunication			ForPowerSupply			Total		
Cluster	Low	Mid	High	Low	Mid	High	Low	Mid	High	Low	Mid	High
1	168.984	355.644	704.772	0.000	0.000	0.000	2.988	2.700	2.592	171.972	358.344	707.364
2	129.384	234.252	525.600	2.592	6.336	4.248	5.976	4.104	4.716	137.952	244.692	534.564
3	91.008	213.372	405.072	10.944	11.628	10.620	7.344	6.156	6.480	109.296	231.156	422.172
4	101.124	177.804	369.864	12.600	12.924	18.792	11.664	8.244	10.008	125.388	198.972	398.664
5	86.508	155.484	311.976	16.488	15.480	17.064	15.264	9.324	13.212	118.260	180.288	342.252
6	69.156	126.936	268.380	17.460	18.324	23.04	17.856	12.780	14.616	104.472	158.04	306.036
7	59.328	114.624	249.984	25.992	23.940	26.892	19.476	17.604	19.080	104.796	156.168	295.956
8	53.496	127.512	214.128	33.588	27.036	30.024	22.860	20.628	18.864	109.944	175.176	263.016
9	47.628	122.184	199.044	34.956	28.260	27.072	22.320	23.940	21.888	104.904	174.384	248.004
10	42.408	97.092	188.172	37.944	32.832	32.112	26.064	25.704	26.136	106.416	155.628	246.420
11	39.744	81.936	187.668	38.628	36.576	36.072	29.448	27.720	31.104	107.820	146.232	254.844
12	37.872	80.352	170.064	41.292	39.240	38.052	34.236	27.936	32.940	113.400	147.528	241.056
13	31.464	76.392	150.984	40.392	39.240	37.620	34.956	32.544	35.388	106.812	148.176	223.992
14	30.888	63.180	132.876	46.728	43.632	40.788	38.664	35.208	36.684	116.280	142.020	210.348

TABLE 10. Comparison of clustering total weight results (in g) across selected routing strategies and application scenarios. The weight for data communication is computed as the sum of Centroids-to-Centroids and Centroids-to-HPC data paths, while the power supply weight is computed from Centroids-to-Battery paths. The total weight combines the components path (avoiding restricted zones), data communication, and power supply according to the application scenario.

Zonal	ComponentsPathAvoidRZ			ForDataCommunication			ForPowerSupply			Total		
Cluster	Low	Mid	High	Low	Mid	High	Low	Mid	High	Low	Mid	High
1	2903.50	6700.24	15632.03	0.00	0.00	0.00	3705.12	3348.00	3214.08	6608.62	10048.24	18846.11
2	2184.51	4477.95	11322.07	13.30	32.50	21.79	5664.60	4527.29	5847.84	7862.41	9037.75	17191.70
3	1753.70	4142.90	8361.33	53.76	57.11	52.44	5952.31	5652.79	8035.20	7759.78	9852.81	16448.97
4	1764.95	3503.97	6759.66	65.83	66.02	92.58	6025.74	7981.20	12409.92	7856.51	11551.19	19262.17
5	1376.86	3122.32	5792.99	83.71	82.73	85.91	5194.36	6677.88	16382.88	6654.92	9882.93	22261.78
6	1086.68	2484.45	4874.88	90.54	96.04	115.31	4543.06	6707.25	17484.26	5720.28	9287.74	22474.45
7	981.54	1936.07	4574.74	132.52	124.85	136.67	4547.06	6572.25	19486.60	5661.13	8633.17	24198.01
8	823.38	2049.63	4177.08	170.83	141.67	153.21	4101.02	6939.35	18772.96	5095.23	9130.65	23103.25
9	761.11	1976.41	3564.31	180.92	148.39	144.64	4044.53	6612.95	18863.91	4986.55	8737.75	22572.86
10	671.18	1661.32	3233.13	197.35	173.44	170.25	4059.14	6557.47	22925.30	4927.66	8392.24	26328.68
11	637.72	1390.23	3215.78	201.07	192.90	190.37	3910.75	5945.28	20573.87	4749.53	7528.41	23980.03
12	534.65	1364.07	2967.78	217.06	208.76	200.88	3121.95	5955.58	19751.99	3873.66	7528.41	22920.65
13	475.48	1195.84	2691.66	216.17	213.27	201.17	3063.40	4946.54	19813.29	3755.06	6355.64	22706.12
14	441.36	991.60	2424.00	248.55	234.86	219.80	3032.84	4839.50	19987.76	3722.74	6065.95	22631.56

Furthermore, the routing explicitly incorporates restricted zones—areas where wiring cannot pass, such as crumple zones and hot engine regions—which increases the total routing length. These restricted zones are standard in modern vehicle designs and are critical for ensuring safety and manufacturability. Finally, the dataset used in this study is unique, provided by project partners, and reflects actual vehicle layouts and constraints. These factors contribute to the higher absolute weight while demonstrating the practical applicability and robustness of the proposed method under realistic conditions.

In addition, Fig. 10 illustrates a qualitative comparison of AI-generated and manually designed routing layouts for the high application scenario. The AI-generated design replicates the manual layout while reducing design time, cost, and weight. Table 9 and Table 10 further detail the clustering-based distance and weight results across different routing strategies and application scenarios.

D. COST EFFICIENCY GAINS OF AI-BASED ROUTING

In addition to improvements in wiring length, weight, and design maturity, the proposed AI-based zonal clustering and routing approach provides measurable cost-efficiency benefits compared to manual methods. Industry reports suggest that traditional manual harness designs realize only about 50% of the potential cost efficiency [50], leaving significant savings unexploited. In our collaboration with project partners, manual routing was performed using spreadsheet-based tools, requiring several weeks to converge to a feasible, yet suboptimal, layout. In contrast, the AI-based method produced an optimized routing in under a week, representing an 80–90% reduction in design time. This reduction in engineering effort directly translates to lower development costs by minimizing labor hours and reducing the number of physical prototypes required. Furthermore, the AI-optimized design produced a leaner harness compared to the manually routed layout for the same subsystem, as shown in Fig. 10 and Table 11. Since material and assembly costs scale with wiring length and weight, the observed reductions directly contribute to cost savings. Even in raw material terms, copper for automotive cables is priced at approximately €1.5 per kilogram [51], so reducing the harness weight by about 5 kg translates to a copper material saving of roughly €7.5 per vehicle—exclusive of additional savings from

TABLE 11. Wiring length and weight comparison with existing methods. Reported results in prior studies assume lower ECU counts and do not consider restricted zones and wire type; thus, absolute values are not directly comparable. Proposed method accounts for realistic ECU counts, vehicle constraints, and restricted-zone-aware routing.

Study	Size (m)	ECUs	Length (m)	Weight (kg)
Park [32]	4.8×2.0	120	100	3.9
Stillig [48]	Large	N/A	1600	60
Park [31] DIA	N/A	60	65.05	2.44
Park [31] ZIA	N/A	60	49.02	1.84
Lee [49]	N/A	150	5000	N/A
Proposed (Low)	4.76×1.85	103	113.4	3.87
Proposed (Mid)	4.76×1.85	206	147.53	7.53
Proposed (High)	4.76×1.85	417	241.06	22.92

insulation, connectors, and assembly labor. Considering typical industry-reported labor and overhead costs, total per-vehicle savings could plausibly reach approximately €150. At high production volumes, such savings accumulate significantly (e.g., €150 per vehicle ×100,000 units = €15 million in total savings). Moreover, a lighter harness contributes to improved vehicle efficiency, either by extending battery range in electric vehicles or reducing fuel consumption and exhaust emissions in internal combustion vehicles [48], thereby providing indirect cost and performance benefits over the vehicle's lifetime.

V. CONCLUSION AND FUTURE WORK

This study demonstrates that an AI-based multi-zonal approach to automotive E/E architecture can significantly optimize wiring length, mass, and design effort while maintaining system functionality. Compared to manually designed layouts, the proposed method achieved measurable improvements in harness efficiency, material use, and estimated cost savings, supported by both quantitative results and qualitative comparisons with existing methods. Across evaluations from 1 to 14 zones (under Low, Mid, and High application loads), an intermediate 12-Zone configuration consistently emerged as the best-balanced solution. The 12-Zone design minimized total harness length (241.056 m) and weight (22.92 kg) compared to both fewer zones (which increase intra-zone wiring) and excessive zones (which add interconnect overhead). This configuration leverages an inter-centroid ring topology for robust data communication between zone controllers and a central high-performance controller, alongside properly gauged battery feed lines sized to each cluster's current draw. Additionally, the AI-based design reduced engineering effort and improved cost efficiency compared to manual methods, offering potential savings at scale. These results validate the benefits of zonal E/E architectures and AI-driven optimization for complex vehicular systems.

Future work will extend the clustering and routing model to dynamic usage scenarios, including: *Summer Sunny Day City Idle Traffic, Winter Sunny Day Highway Traffic, Winter Rainy Night City Idle Traffic, Summer Rainy Night Highway Traffic*. These use cases represent diverse driving and environmental conditions, allowing assessment of the architecture's performance under varying thermal and load profiles. Additionally, a CO_2 emission (g/m) based cluster optimization will be pursued, integrating environmental impact into the design. By correlating harness weight with vehicle fuel/energy consumption, this optimization aims to further reduce the carbon footprint of future zonal E/E architectures. A current limitation of the study is that the routing simulation relies on 2D coordinate data, which simplifies real-world geometry; extending to 3D spatial models will improve routing accuracy and applicability to complex vehicle platforms such as EVs and autonomous vehicles.

ACKNOWLEDGMENT

This research is funded by the German Federal Ministry of Education and Research (BMBF) under grant number 16ME0783, within the KI4BoardNet project (''Integral Agile E/E Development for Fusion and Standardized Power and Data Wiring Systems'') as part of the funding initiative ''Electronics and Software Development Methods for the Digitalization of Automobility.'' The authors gratefully acknowledge the collaboration and support of project partners EDAG Engineering and KROSCHU GmbH Germany for their technical contributions and coordination support. Project coordination is led by CARIAD SE. More information is available at [44].

DATA AVAILABILITY STATEMENT

The data supporting the findings of this study are confidential and cannot be shared publicly due to industrial collaboration agreements and data security requirements.

CONFLICT OF INTEREST

The authors declare no conflict of interest.

REFERENCES

[1] K. Eder, O. Tas, J. Neckenich, R. Winter, U. Zielbauer, and K. Paetzold, ''Knowledge reuse of CAD data in parallel development of multiple wiring harness variants,'' in *Proc. Int. Conf. Adv. Syst. Eng.*, 2023, pp. 196–205.

[2] J. Maier and H.-C. Reuss, ''Design of zonal E/E architectures using k-means clustering and Dijkstra's algorithm,'' *Energies*, vol. 16, no. 19, p. 6884, 2023.

[3] J. Maier and H.-C. Reuss, ''Handling system complexity in zonal E/E architectures,'' *Transp. Eng.*, vol. 13, Sep. 2023, Art. no. 100195.

[4] H. Jang, C. Park, S. Goh, and S. Park, ''Design of a hybrid in-vehicle network architecture combining zonal and domain architectures for future vehicles,'' in *Proc. IEEE 6th Int. Conf. Knowl. Innov. Invention (ICKII)*, Aug. 2023, pp. 33–37.

[5] C. Cui, C. Park, and S. Park, ''Physical length and weight reduction of humanoid in-robot network with zonal architecture,'' *Sensors*, vol. 23, no. 5, p. 2627, Feb. 2023.

[6] J. Lim, J. Lee, Y. S. Hong, and C. Kang, ''A framework for designing zonal architectures for in-vehicle networks: Balancing communication load and wiring length,'' *IEEE Trans. Veh. Technol.*, vol. 74, no. 5, pp. 7940–7952, May 2025.

[7] H. M. Kadry, A. Gupta, J. Lawlis, and M. Volpone, ''Electrical architecture and in-vehicle networking: Challenges and future trends,'' in *Proc. IEEE Int. Symp. Circuits Syst. (ISCAS)*, May 2022, pp. 1009–1013.

[8] C. Gopinath and M. Thenmozhi, ''Ai-optimized electrical wiring harness design for automotive applications (Connector Selection), in *Challenges in Information, Communication and Computing Technology*, 1st ed. CRC Press, 2024, pp. 543–549.

[9] R. Arvind, "Design and development of Ai-based wiring harness simulator for pigtail wiring harness development in electrical checkout system (ECOS)," *Int. J. Adv. Res. Sci., Commun. Technol. (IJARSCT)*, vol. 4, no. 2, pp. 284–290, Jul. 2024.
[10] T. Karlsson, E. Åblad, T. Hermansson, J. S. Carlson, and G. Tenfält, "Automatic cable harness layout routing in a customizable 3D environment," *Comput.-Aided Des.*, vol. 139, 2024, Art. no. 103671.
[11] A. Prabhakaran, P. Thirumoorthi, and K. S. D. Krishnan, "Design and development of an intelligent zone based master electronic control unit for power optimization in electric vehicles," *Sci. Rep.*, vol. 14, no. 1, p. 20142, Aug. 2024.
[12] B. Y. Suprapto, J. Jonathan, and S. Dwijayanti, "Implementation of the A* algorithm for autonomous electric vehicle routing," in *Proc. Int. Workshop Artif. Intell. Image Process. (IWAIIP)*, Dec. 2023, pp. 304–308.
[13] H. Liu, T. Shan, and W. Wang, "Automatic routing study of spacecraft cable based on A-star algorithm," in *Proc. IEEE 5th Inf. Technol. Mechatronics Eng. Conf. (ITOEC)*, Jun. 2020, pp. 716–719.
[14] K. Kim, Y. Yoon, B. C. Kim, J. Kim, S. Han, and S. Kwon, "Automatic cable routing with b-spline optimization for collision avoidance," *J. Comput. Design Eng.*, vol. 11, no. 5, pp. 303–317, 2024.
[15] P. Heisler, P. Steinmetz, I. S. Yoo, and J. Franke, "Automatization of the cable-routing-process within the automated production of wiring systems," *Appl. Mech. Mater.*, vol. 871, pp. 186–192, 2017.
[16] X. Liu, Y.-L. Chen, L. Y. Por, and C. S. Ku, "A systematic literature review of vehicle routing problems with time windows," *Sustainability*, vol. 15, no. 15, 2023. [Online]. Available: https://www.mdpi.com/2071-1050/15/15/12004
[17] T. Gaon, Y. Gabay, and M. Weiss Cohen, "Optimizing electric vehicle routing efficiency using K-means clustering and genetic algorithms," *Future Internet*, vol. 17, no. 3, p. 97, Feb. 2025.
[18] X. Wu, G. Wang, and N. Shen, "Obstacle avoidance optimization and path planning of autonomous vehicles using attention mechanisms," *Frontiers Neurorobotics*, vol. 17, Jan. 2023, Art. no. 1269447.
[19] L. Wang and Z. Liu, "Data-driven product design evaluation method based on multi-stage artificial neural network," *Appl. Soft Comput.*, vol. 103, May 2021, Art. no. 107117.
[20] I. Khan, F. Khan, A. Ali, B. Alshawi, R. Alturki, and M. Wedyan, "Secure and optimized clustering in VANETs," in *Proc. Int. Conf. Electr., Comput. Energy Technol. (ICECET)*, Mar. 2024, pp. 1–6.
[21] T. Gaon, Y. Gabay, and M. W. Cohen, "Optimizing ev routing with k-means clustering and genetic algorithms," *Future Internet*, vol. 17, no. 3, p. 97, 2025.
[22] H. Wang and R. Johansson, "Deep learning-based connector detection for robotized assembly of automotive wire harnesses," in *Proc. IEEE 19th Int. Conf. Automat. Sci. Eng. (CASE)*, 2023, pp. 1–8.
[23] C. Wang, R. Zhang, R. Hong, and H. Wang, "Attention-enhanced deep reinforcement learning for electric vehicle routing optimization," *IEEE Trans. Transp. Electrific.*, p. 1, 2025.
[24] X. Jiang, Y. Nagaoka, K. Ishii, S. Abiko, T. Tsujita, and M. Uchiyama, "Robotized recognition of wire harnesses via tracing," *Robot. Comput.-Integr. Manuf.*, vol. 34, pp. 52–61, Jan. 2015.
[25] C. Bianchi, R. Merlino, and R. Passerone, "Combining optimization and simulation for off-road vehicle E/E design," *Sensors*, vol. 24, no. 15, p. 4889, 2024.
[26] E. Nagy, "Design factors for electric vehicle power distribution systems," in *Proc. 3rd Cognit. Mobility Conf.*, Cham, Switzerland. Springer, 2025, pp. 300–313.
[27] A. T. Jacob and N. Mahiban Lindsay, "Designing EV harness using autocad electrical," in *Proc. 8th Int. Conf. Smart Struct. Syst. (ICSSS)*, Apr. 2022, pp. 1–4.
[28] J. Dou, X. Dai, and Z. Meng, "Graph theory-based optimization of flow-line configurations," *Int. J. Adv. Manuf. Technol.*, vol. 41, nos. 9–10, pp. 916–931, 2009.
[29] C. Park, C. Cui, and S. Park, "Analysis of E2E delay and wiring harness in in-vehicle network with zonal architecture," *Sensors*, vol. 24, no. 10, p. 3248, May 2024.
[30] C. Bianchi, R. Merlino, and R. Passerone, "Combining optimization and simulation for next-generation off-road vehicle e/e architectural design," in *Proc. Sensors*, vol. 24, no. 15, Basel, Switzerland, 2024, p. 4889.
[31] C. Park and S. Park, "Performance evaluation of zone-based in-vehicle network architecture," *Sensors*, vol. 23, no. 2, p. 669, 2023.
[32] C. Park, C. Cui, and S. Park, "Analysis of E2E delay and wiring harness in zonal architecture," *Sensors*, vol. 24, no. 10, p. 3248, 2024.
[33] D. Stöhrmann, A. Kostrzewa, R. Ernst, and H. Kellermann, "Towards OFDMA-based Ethernet for future in-vehicle communication," in *Proc. 2nd Int. Conf. Societal Autom. (SA)*, May 2021, pp. 1–8.
[34] N. Sperling and R. Ernst, "Reducing communication cost and latency in autonomous vehicles with subscriber-centric selective data distribution," in *Proc. IEEE 99th Veh. Technol. Conf. (VTC-Spring)*, Jun. 2024, pp. 1–7.
[35] K. Appajosyula, "Ethernet-based IDS for zonal architecture," SAE Tech. Paper 2024-28-0121, 2024.
[36] S. S. Shetiya, V. Vyas, and S. Renukuntla, "Zonal architecture development with evolution of artificial intelligence," 2024, *arXiv:2412.01840*.
[37] H. Iqbal, D. Campo, M. Baydoun, L. Marcenaro, D. M. Gomez, and C. Regazzoni, "Clustering optimization for abnormality detection in semi-autonomous systems," in *Proc. 1st Int. Workshop Multimodal Understand. Learn. Embodied Appl.*, Oct. 2019, pp. 33–41.
[38] S. S. Shetiya, V. Vyas, and S. Renukuntla, "Zonal architecture development with evolution of artificial intelligence," 2024, *arXiv:2412.01840*.
[39] M. Bornemann. (2021). *Zone Controllers Build Bridge to Tomorrow's Technology*. Aptiv. Accessed: Jul. 4, 2025. [Online]. Available: https://www.aptiv.com/docs/default-source/white-papers/2021_aptiv_whitepaper_zonecontroller.pdf?sfvrsn=c1f9163d_23
[40] P. Aberl, S. Haas, and A. Vemuri. (2021). *How a Zone Architecture Paves the Way to a Fully Software-Defined Vehicle*. Texas Instruments. Accessed: Jul. 4, 2025. [Online]. Available: https://www.ti.com/lit/wp/spry345a/spry345a.pdf
[41] H. G. Nguyen, M. Kuhn, and J. Franke, "Manufacturing automation for automotive wiring harnesses," *Proc. CIRP*, vol. 97, pp. 379–384, Jan. 2021.
[42] H. Askaripoor, M. Hashemi Farzaneh, and A. Knoll, "E/E architecture synthesis: Challenges and technologies," *Electronics*, vol. 11, no. 4, p. 518, Feb. 2022.
[43] P. Larrenie, J.-F. Bercher, O. Venard, and I. Lahsen-Cherif, "Low complexity adaptive machine learning approaches for end-to-end latency prediction," 2023, *arXiv:2301.13536*.
[44] Edacentrum. *KI4BoardNet Project Overview*. Accessed: Jul. 31, 2025. [Online]. Available: https://www.edacentrum.de/ki4boardnet/
[45] G. Hamerly and C. Elkan, "Learning the K in K-means," in *Proc. Adv. Neural Inf. Process. Syst.*, vol. 16, 2003, pp. 281–288.
[46] J. Lian, C. Cui, W. Sun, Y. Wu, and R. Huang, "KD-RRT: Restricted random testing based on K-dimensional tree," in *Proc. 8th Int. Conf. Dependable Syst. Their Appl. (DSA)*, 2021, pp. 590–599.
[47] R. F. Sproull, "Refinements to nearest-neighbor searching ink-dimensional trees," *Algorithmica*, vol. 6, nos. 1–6, pp. 579–589, Jun. 1991.
[48] J. Stillig and N. Parspour, "Novel infrastructure platform for a flexible and convertible manufacturing," *Adv. Sci., Technol. Eng. Syst. J.*, vol. 6, no. 1, pp. 356–368, Jan. 2021.
[49] T. Lee. (2020). *The Sense-Think-Act Model of Autonomous Vehicles*. Accessed: Jul. 6, 2025. [Online]. Available: https://www.microcontrollertips.com/the-sensethink-act-model-of-autonomous-vehicles-faq/
[50] Wiring Harness News. (2025). *Harness Manufacturing and the Consequences of Software Defined Vehicles*. Accessed: Jul. 2025. [Online]. Available: https://wiringharnessnews.com/harness-manufacturing-and-the-consequences-of-software-defined-vehicles/
[51] BEDIA Kabel. (2025). *Copper Calculation–Customer Information*. Accessed: Jul. 2025. [Online]. Available: http://www.bedia-kabel.de/en/webshop/customer-information/copper-calculation.html

MD SANOWAR HOSSAIN was born in Jashore, Bangladesh, in 1982. He received the B.Sc. degree in electronics and communication engineering from Khulna University, Bangladesh, in 2007, the M.B.A. degree from East West University, Dhaka, in 2016, and the M.Sc. degree in information engineering and computer science from the Rhine-Waal University of Applied Sciences, Kamp-Lintfort, Germany, in 2022. He is currently pursuing the Ph.D. degree with the Institute of Intelligent Cyber-Physical Systems (ICPS), Heilbronn University of Applied Sciences, Germany.

He began his professional career as a Telecommunication Engineer in radio and transmission at Fair and Appropriate Technology Ltd., Dhaka, from 2007 to 2009. He then joined Robi Axiata Ltd., a multinational telecommunications company, where he served in various roles, including a Specialist in core and radio network, from 2009 to 2015, and the Manager of core, radio, and transmission networks, from 2015 to 2019. Since 2023, he has been a Research Assistant in the KI4BoardNet Project funded by BMBF. He earned the TensorFlow Developer Certificate, in 2024. His research interests include AI-driven harness optimization, zonal E/E architecture, automotive data communication, and system-level design for autonomous vehicles.

Mr. Hossain received several recognitions, including the Outstanding Performance Award, in 2018, the Guiding Principles Champion Award, in 2017, and the Talent Council Award, in 2015, along with an international learning opportunity in Malaysia, in 2014, during his tenure.

HAFIZ ABDUL QUDDUS was born in Sialkot, Pakistan, in 1995. He received the B.S. degree in software engineering from the University of Sargodha, in 2018, and the M.Phil. degree in computer science from Quaid-i-Azam University (QAU), Islamabad, Pakistan, in 2022. He is currently pursuing the Ph.D. degree with the Institute of Intelligent Cyber-Physical Systems (ICPS), Heilbronn University of Applied Sciences, Germany. He was a Research Assistant with HEC Pakistan-funded project, from 2020 to 2021, and a Teaching Assistant with the CS Department, QAU, from 2021 to 2022. He was awarded a gold medal and merit certificate for his M.Phil. research. He is a Research Assistant in the KI4BoardNet Project funded by German BMBF. His research interests include formal methods, and symbolic and subsymbolic AI techniques for verifying hardware/software systems and designs.

ZIYA CEVAHIR was born in Bad Mergentheim, Germany. He received the B.S. degree in electrical engineering and the M.S. degree from the Heilbronn University of Applied Sciences, Künzelsau, Germany, in 2017 and 2019, respectively. From 2019 to 2023, he was an External Lecturer at Heilbronn University, where he taught a course on communication technologies with a focus on information theory, source coding, and channel coding. In parallel, he has been employed as an Engineer in electronic development at ebm-papst Mulfingen GmbH & Company KGaA & Company KG. Since 2023, he has been a Research Assistant in the KI4BoardNet Project funded by German Federal Ministry of Education and Research (BMBF) at the Institute of Intelligent Cyber-Physical Systems (ICPS), Heilbronn University of Applied Sciences. His research interests include robust and intelligent communication systems leveraging artificial intelligence techniques.

ALEXANDER JESSER was born in Kazakhstan. He received the Diploma degree in computer engineering from the University of Paderborn, Germany, and the Ph.D. degree in computer engineering from the Johann Wolfgang Goethe University of Frankfurt a.M., Germany. Since 2013, he has been a Full Professor of embedded systems and communications engineering at Heilbronn University, Germany. Prior to his academic career, he worked in leading positions with companies in the medical technology field and in the automotive industry. In 2021, he founded the Institute of Intelligent Cyber-Physical Systems (ICPS, www.hs-heilbronn.de/icps) and has headed it ever since. He was also a Visiting Professor at Paraguayan German University (UPA), Asunción, Shenzhen University of Technology (SZTU), and Dulaty University, Kazakhstan. In 2024, he was awarded the additional title of a Professor at the UPA due to his extraordinary relationships. He is conducting research in the field of cyber-physical systems, signal-, image-, and voice processing in industrial, and medical technology applications. Besides this, he is represented on several international scientific committees, such as RICOTED.